Chapter-3

Experimental Investigations of Cyclone Separator for Syngas Production and Effect of Blending with Biodiesel on Emission

In this chapter, we discuss on dust particle removal, which is present in producer gas by a cyclone separator. Also, discussion on the degradation of biodiesel calorific value with storage time. In §3.1 we present a brief introduction. We then present the working principle of cyclone separator in §3.2. In section §3.3, we discuss on the cyclone performance parameters. We report cyclone performance evaluation in §3.4 followed by the experimental method in §3.4.1 which is compared with numerical Leith and Licht model in 3.4.2. In section §3.5, we briefly discuss on biodiesel. We then discuss on biodiesel manufacturing by transesterification in §3.5.1 along with storage time in §3.5.2. We then discussion on biodiesel quality measuring parameters §3.5.3 and instruments used for experiments §3.5.4. In section §3.6 we present the biodiesel production procedure, viscosity of biodiesel §3.6.1, calorific value of biodiesel §3.6.2 and variable compression ratio (VCR) research test setup §3.6.3. Laboratory experiments are described in §3.7. Conclusions are discussed in §3.8.

3.1 Introduction

The fuel used for gasification contains mineral compositions which are oxidised during combustion and pyrolysis called ash, along with ash there are tar and char particles also mixed with syngas. Syngas is a mixture of combustible gases like- H_2, CO and CH_4 and it is the purest form of producer gas which can be directly used as a gaseous fuel for running the dual-fuelled Internal Combustion Engines. Dust production is shown in figure 3.1 as a function of gas production [1]. Dust particle size and concentration depend on the type of feedstock, operating conditions and gasifier type etc. Generally, producer gas is used as a gaseous fuel to run the dual-fuelled IC engine for power generation. So, before using producer gas, ash and char particulates should be removed to ensure the proper functioning of the system. According to Hasler et al. [2], acceptable particle size in the producer gas which is used as a fuel for *IC* engine and gas turbine should be less than 10 and 5 microns respectively, so those particles having a greater size than mentioned, needs to be removed. Although, there are so many filters like- filter bags,

cyclone separators, scrubbers, precipitators etc. are available to remove dust particle but still, the selection of the filtration system is based on the utilisation of producer gas. The general efficiency of these filtration systems is shown in Table 3.1.

In connection of the above, the overall efficiency of the dual-fuelled diesel engine increases when filtered producer gas is supplied together with the diesel as a fuel. The experimental setup cyclone separator is an inbuilt part of the gasifier system work for dust filtration. So, cyclone separator performance has been evaluated by using different methods which are discussed in the cyclone performance evaluation section.

On the other hand, when the producer gas quality is not up to the mark, the overall engine efficiency also reduces. Hence, blending of biodiesel with conventional diesel comes into the picture and compensate the deficiency of producer gas. But, before bio-diesel use, it is essential to know how long bio-diesel can be stored and what are the emissions that comes out when it is blended with the conventional diesel.

In connection of the above, we have performed the experiments on Soyabean bio-diesel for analysis of the degradation of the quality of Soyabean bio-diesel with storage time and its emissions on various loads. Based on results, in future, one can use this bio-diesel and producer gas simultaneously as a fuel to run the dual-fuelled diesel engine, which may result in reduction in considerable amount of conventional diesel.

Table 3.1: Efficiency of different technologies for removal of particles [3].

Method	Temperature range (^{o}c)	Efficiency
Cyclone	100-900	Particles>5 µm 80%
Wet scrubbers (venture)	20-100	Particles>0.1-1µm 85-95%
Rigid ceramic filter	200-800	Particles>0.1µm 99.5-99.9%

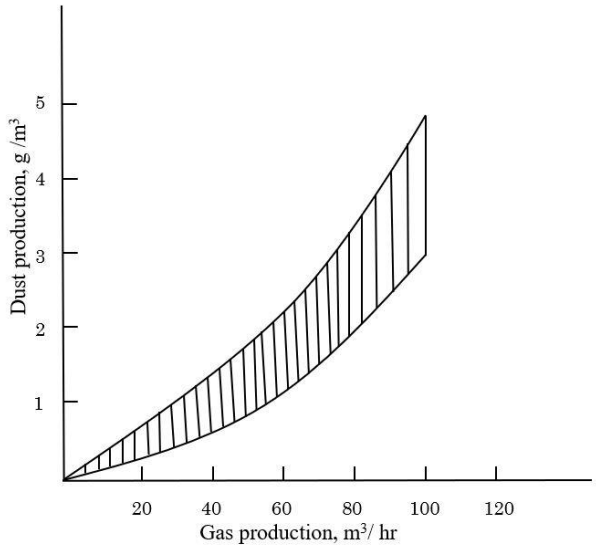

Figure 3.1: Dust production v/s Gas production [1]

3.2 Working principle of cyclone separator

Cyclone separator works on the principle of separation of particles due to centrifugal force and gravity. At high inlet velocity, the mixture of fluid and particles enters through the tangential inlet, due to shape of cyclone separator this mixture rotates and form a vortex. The particles having a higher density than fluid can't follow curve vortex path due to inertia, and therefore, they strike with the outer wall of the cyclone and due to gravity heavy particles settle down at the bottom of the cyclone.

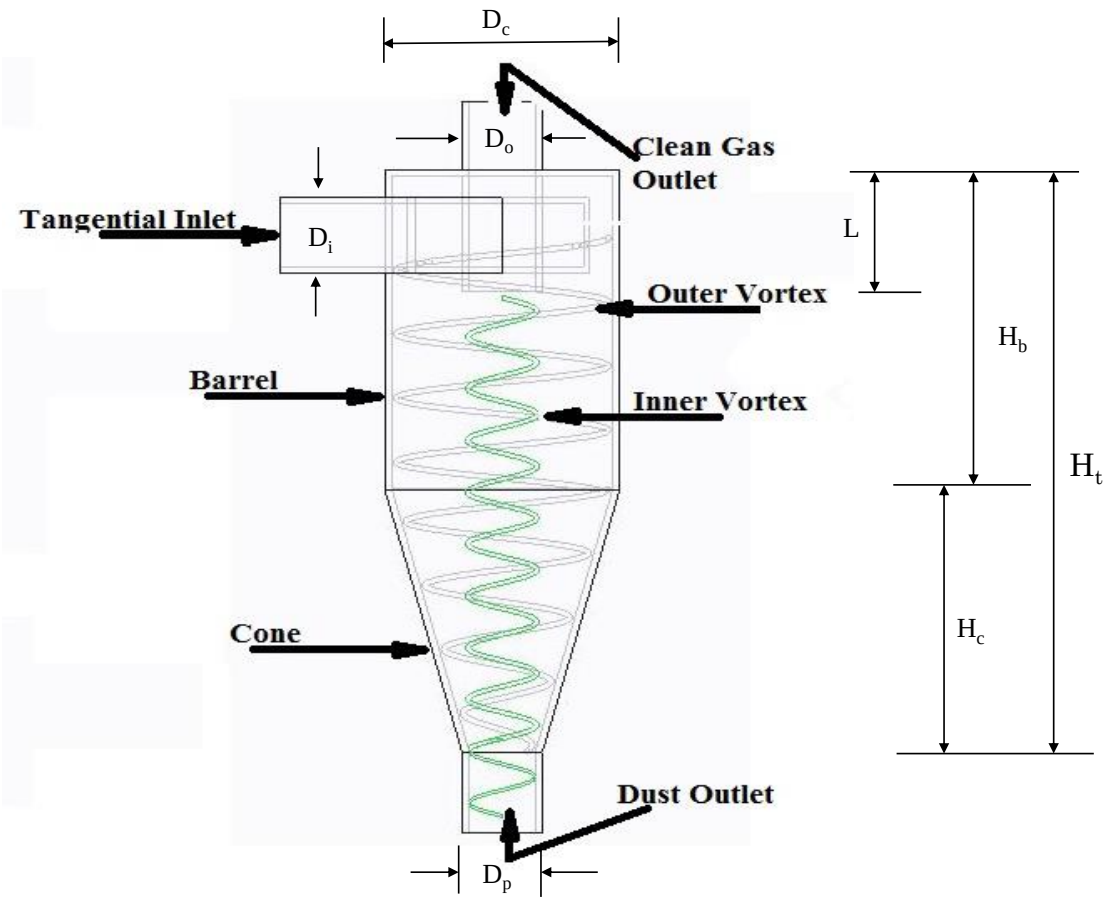

Figure 3.2: Schematic of cyclone separator.

Cleaned gas goes outside through outlet provided at the upper side of a cyclone after forming inner vortex inside cyclone separator. As shown in figure 3.2, cyclone has an upper cylindrical part called barrel and bottom conical portion, as the stream goes in a downward direction through conical portion more smaller particles strikes with cyclone wall and settle down at the bottom. As a result, collection efficiency increases. [4]

Following forces play a significant role to separate the particle in the cyclone separator, which is described below:[5]

I. Buoyant force opposes particle outward motion this is due to density difference between particle and fluid.

$$F_b = -\frac{4\pi r_p^3}{3}\rho_f \frac{V_t^2}{r} \tag{3.1}$$

II. Drag force opposes outward motion of particle this is due to viscous force between fluid and particles.

$$F_d = -6\pi r_p \mu V_r \tag{3.2}$$

III. Centrifugal force moves particle outward.

$$F_c = \frac{4}{3} \times \pi \times \rho_p \times r_p^3 \times \frac{V_t^2}{r} \tag{3.3}$$

The outward radial speed of each particle is determined by setting Newton's second law of motion equal to the sum of these forces.

Resultant force:

$$m \frac{dV_r}{dt} = F_d + F_c + F_b \tag{3.4}$$

where;

m = mass of particles

r_p = radius of particle

ρ_f = density of fluid

V_t = tangential inlet velocity

r = radius of cyclone separator

ρ_p = density of particle

V_r = radial velocity

3.3 Cyclone performance parameter

Cyclone performance generally measure by:

a) Collection efficiency:

Collection efficiency shows that how much particle does cyclone capable of removing from the stream of fluid. Theoretically, cyclone removes all particles having diameter more than cut-size diameter; this is shown in figure 3.3. Cut size

diameter is a particle diameter for which particle experiences no resultant force, it is in equilibrium (Centrifugal force = Buoyant force + Drag force). These particles have a 50% probability of settling down and of escaping out with fluid. [6]

b) Pressure drop:

Pressure drop shows energy loss in the cyclone hence, cyclone separator should be designed for the low-pressure drop or less energy loss. As the cyclone diameter decreases, efficiency and pressure drop increases, therefore, for better performance both parameters need to be optimized. Efficiency and pressure drop depends on cyclone dimensions (cyclone diameter, vortex finder diameter), operating conditions (pressure, temperature) and inlet velocity [6].

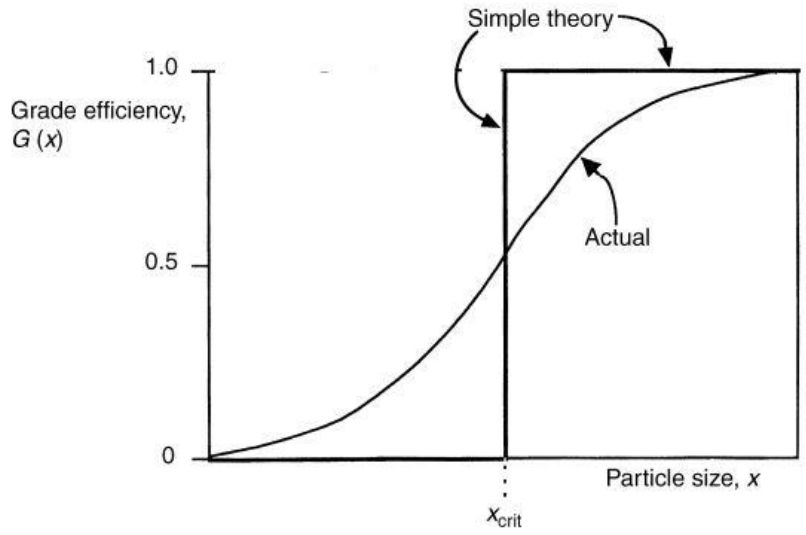

Figure 3.3: Theoretical and actual grade efficiency curve [7].

3.4 Cyclone performance evaluation

To remove the dust particles from the producer gas, using cyclone separator is the best option; therefore, we have investigated the cyclone separator performance in two ways.

3.4.1 Experimental method:

Figure 3.4 shows the photograph of cyclone separator which is an inbuilt part of the existing experimental gasifier system for separating dust particles from the producer gas. When the gasifier system starts producing quality gas, blower sucks the gas and supplied to the inlet of the cyclone separator. Filter paper collects the dust particles by placing at the gas inlet of the cyclone separator for one minute and same for gas outlet, in the meantime, velocity, temperature and pressure drop also measured by using anemometer (range 0.1 to 99.9 *km/h*), digital thermometer (range -30 to 3000°C), and *U* tube manometer respectively. An optical microscope was used for analysing the particle size (maximum and minimum) and the approximate mean value. Particle size distribution was assumed according to normal log law. The viscosity of gas has been calculated using the general equation for the multi-component system [8].

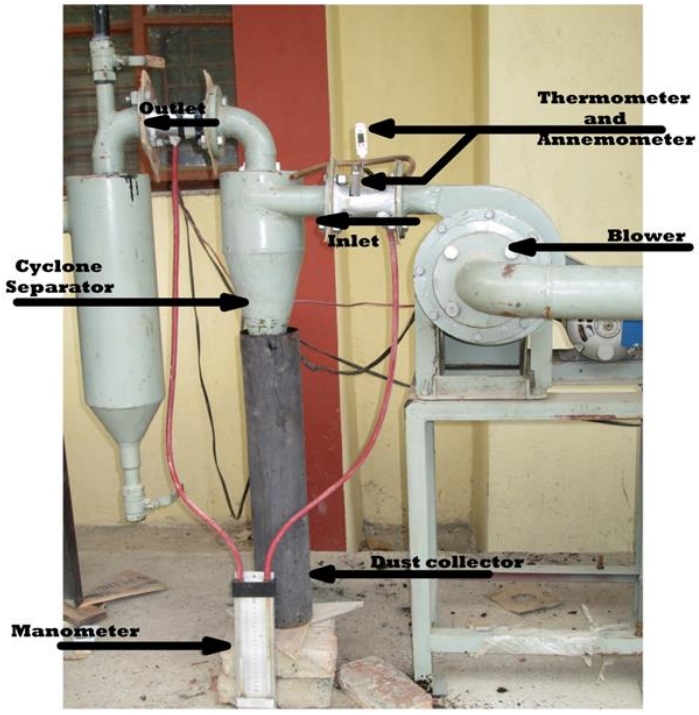

Figure 3.4: Cyclone separator in-built with gasifier system.

Table 3.2: Input parameters of cyclone separator.

Input Parameters used	Dimensions/Units
Cyclone body diameter (D_c)	200 mm
Tangential inlet diameter (D_i)	50 mm
Gas outlet diameter (D_o)	30 mm
Particles outlet diameter (D_p)	25 mm
Vortex finder length (L)	150 mm
Barrel height (H_b)	200 mm
Cylinder height (H_c)	350 mm
Total height (H_t)	550 mm

a) Instrumentation:

Following equipment are used for measuring the input parameters of cyclone separator.

Figure 3.5: Photograph of anemometer to measure the velocity of gas flowing through pipe.

Figure 3.6: Photograph of digital temperature indicator to measure the temperature of gas flowing through pipe.

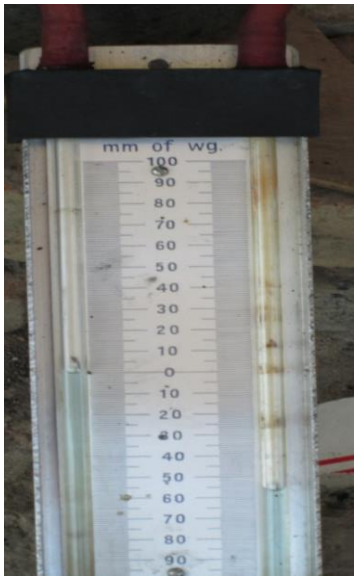

Figure 3.7: Photograph of U-tube manometer to measure the pressure drop across the cyclone separator.

- **Blower:**

  It sucks syngas from reactor and gives feed to cyclone separator.

  Blower specification;

  - Centrifugal Motor
  - Speed: 1425 rpm
  - 220/230V 1φ - Single phase 50Hz
  - Starting capacitance: 100 µF
  - Power: 0.5 HP

b) Observations and calculations:

Following formulas used for calculating the cyclone performance parameters.

- **Cyclone collection efficiency;**

$$\eta = 1 - \frac{M_o}{M_i} \qquad (3.5)$$

where;

M_o = weight of ash collected at outlet, (gm).

M_i = weight of ash collected at inlet, (gm).

- **Pressure drop;**

$$\Delta p = \left(\rho_k - \rho_g\right) \times g \times h \tag{3.6}$$

where;

ρ_k = density of kerosene, (810 kg/m^3).

ρ_g = density of gas, (kg/m^3)

g = gravitational acceleration, (m/s^2)

h = manometric height, (mm)

V_o = inlet flow rate, (m^3/s)

T = temperature, (K)

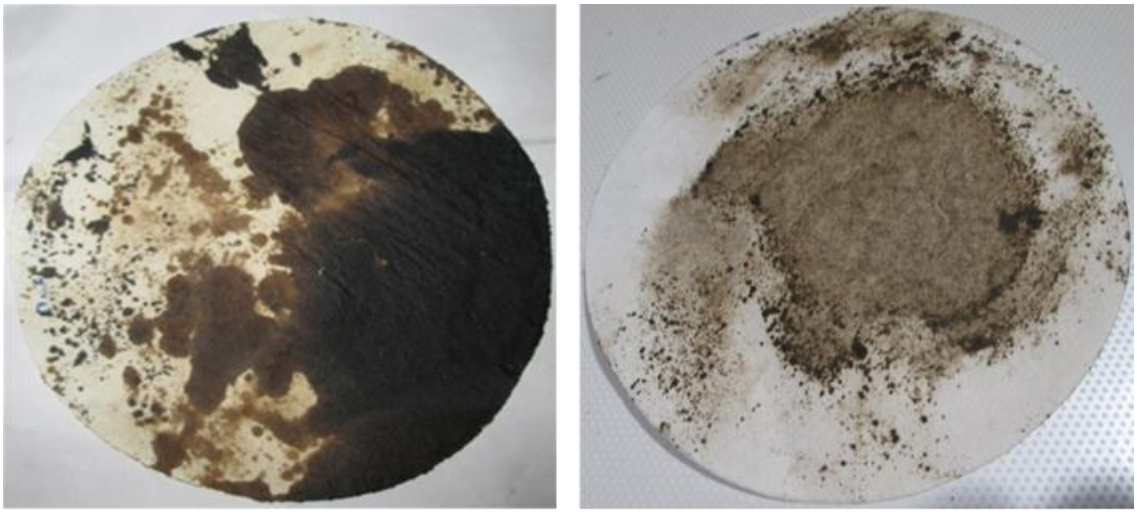

(a) (b)

Figure 3.8: (a) Filter paper containing ash particles at inlet. (b) Filter paper containing ash particles at outlet.

Following data were recorded while conducting experiments on inbuilt cyclone separator for filtration of producer gas having different particle size when wood and coconut shell feedstocks used as a solid fuel for the gasifier system. Moreover, different particle size efficiency also calculated and summarised in Table 3.3.

- **For feedstock - Wood;**

M_i = 0.4620 gm M_o = 0.1300 gm T = 47^0C

Q = 0.028 m^3/s η = 71.86 % Δp = 64.8 Pa

- **For feedstock – Wood with 10 wt.% CaO;**

M_i = 0.2393 gm M_o = 0.07 gm T = 40.4^0C

Q = 0.016 m^3/s η = 70.75 % Δp = 81 Pa

- **For feedstock - Coconut shell;**

M_i = 0.3752 gm M_o = 0.0823 gm T = 40.7^0C

Q = 0.013 m^3/s η = 78 % Δp = 89.1 Pa

- **For feedstock – Coconut shell with 10 wt. % CaO;**

M_i = 0.3502 gm M_o = 0.093 gm T = 39^0C

Q = 0.00989 m^3/s η = 73.44 % Δp = 72.9 Pa

Table 3.3: Particle size efficiency for different feedstocks, (Experimental).

Particle diameter (m)	Efficiency (η) %, Wood	Efficiency (η) %, Wood + 10 wt.% CaO.	Efficiency (η) %, Coconut shell	Efficiency (η) %, Coconut shell + 10 wt.% CaO.
Below $5.00x10^{-06}$	0	0	0	0
$5.00x10^{-06}$	12.88	18.91	31.55	19.27
$10.00x10^{-06}$	56.00	60.36	68.93	66.30
$15.00x10^{-06}$	88.91	89.71	92.65	95.20
$20.00x10^{-06}$	98.50	98.45	98.57	99.65
Above$20.00x10^{-06}$	100	100	100	100

3.4.2 Using Leith and Licht model

This model takes temperature into account and provides the pressure drop, cut-diameter and the separation efficiency of particle diameter d_p. Leith and Liche added the following assumption for particle motion at entry and collection region [9].

- The tangential velocity of particle and gas are equal, therefore, no-slip in the tangential direction between gas flow and particle.

- The relation between the tangential velocity and radius is described by:

  $V_t \times R^n$ = constant.

  where:

  V_t = tangential velocity (m/s)

  n = constant

  R = radius (m)

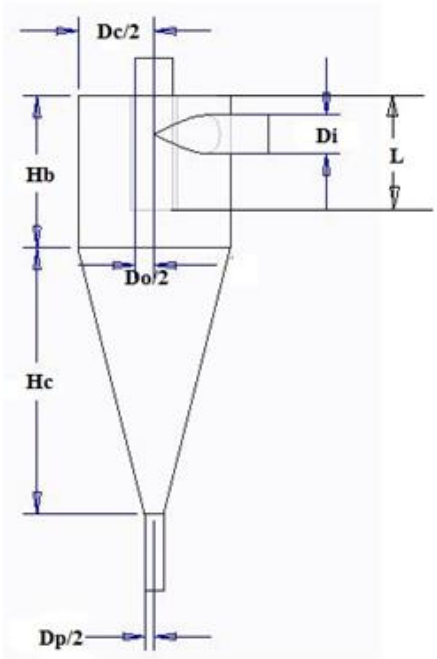

Figure 3.9: Schematic of cyclone separator [9].

a) Observations and calculations:

Following empirical equations are used for calculating the cyclone performance parameters.

- **For efficiency of particle diameter (d_p);**

$$\eta = 1 - \exp\left[-2 \times \left(\left[\frac{G \times \tau \times V_0}{D_c^3} \times (n+1)\right]^{\frac{0.5}{n+1}}\right)\right] \quad (3.7)$$

where,

$$G = \frac{4 \times D_c \times (2 \times V_S + V)}{\frac{\pi}{4} \times D_i^2} \quad (3.8)$$

$$\tau = \frac{\rho_p \times {d_p}^2}{18 \times \mu} \quad (3.9)$$

$$n = 1 - \left[1 - 0.67 \times \left({D_c}^{0.14}\right)\right] \times \left(\frac{T}{283}\right)^{0.3} \quad (3.10)$$

$$V = \frac{\pi}{4} \times D_c^2 \times (H_b - L) + \frac{\pi}{4} \times D_c^2 \times \left(\frac{Z_c + L - H_b}{3}\right) \times \left(1 + \frac{d_c}{D_c} + \frac{d_c^2}{D_c^2}\right) - \frac{\pi}{4} \times D_o^2 \times Z_c \quad (3.11)$$

$$Z_c = 2.3 \times D_0 \times \left(\frac{D_c^2}{\frac{\pi}{4} \times D_i^2}\right)^{\frac{1}{3}} \quad (3.12)$$

$$d_c = D_c - \left(D_c - D_p\right) \times \left(\frac{L + Z_c - H_b}{H - H_b}\right) \quad (3.13)$$

Secondary flow (V_S); The secondary flow is held between the outside vortex and cover plate along with the boundary layer. In this flow, particles within the boundary layer are escaped out through cyclone outlet without being separate from the secondary flow.

$$V_S = \frac{\pi}{4} \times \left(L - \frac{D_i}{2}\right) \times \left({D_C}^2 - {D_0}^2\right) \quad (3.14)$$

- **For pressure drop:**

  In the cyclone design assessment, the pressure drop is considered as a primary need; also, it is directly proportional to the energy requirement, designing a fan system requires knowledge of the pressure drop through a cyclone. Shepherd and Lapple (1939) described the components where pressure drops [10]:

  - In the inlet section, due to gas expansion.
  - In the cyclone chamber, losses due to wall friction and kinetic energy of rotation.

- Loss of pressure energy due to rotational kinetic energy at any regain.

According to their theoretical investigations, Shepherd and Lapple (1939) developed an empirical model to an evaluation of cyclone pressure drop.

$$\Delta P = \frac{1}{2} \times \rho_g \times V_i^2 \times K \times \frac{\left(\frac{\pi}{4} \times D_i^2\right)}{D_o^2} \quad (3.15)$$

where,

K = Constant, depending on operating conditions and cyclone configurations. It is lies between 12 to 18 for tangential entry cyclone.

D_c = cyclone body diameter, (m)

D_i = tangential inlet diameter, (m)

D_o = gas outlet diameter, (m)

D_p = particles outlet diameter, (m)

G = It is related to the cyclone configuration, (-)

H_t = total height, (m)

H_b = barrel height, (m)

H_c = cylinder height, (m)

L = vortex finder length, (m)

T = temperature, (K)

d_c = cyclone central axis diameter, (m)

d_p = particle diameter, (m)

N = It is related to the vortex coefficient, (-)

ρ_p = particle density, (kg/m^3)

ρ_g = gas density, (kg/m^3)

M = viscosity of fluid, (Pa s)

V = volume from where the vortex turns, (m^3)

V_i = inlet gas velocity, (m/s)

V_S = secondary volumetric flow rate, (m^3/s)

V_O = inlet volumetric flow rate, (m^3/s)

Z_C = natural length, (m)

H = cyclone separation efficiency, (-)

T = relaxation time, (sec.)

b) Viscosity of producer gas:

Producer gas is a mixture of multiple gases components like- *CO_2, CO, H_2, CH_4, NO, N_2, HC, O_2*. Given equations are used for calculating the viscosity for a mixture of any number of components [8].

$$\mu_m = \frac{\mu_1}{1+\left(\frac{x_2}{x_1}\right)\emptyset_{12}+\left(\frac{x_3}{x_1}\right)\emptyset_{13}+\cdots} + \frac{\mu_2}{1+\left(\frac{x_1}{x_2}\right)\emptyset_{21}+\left(\frac{x_3}{x_2}\right)\emptyset_{23}+\cdots} + \cdots \quad (3.16)$$

The general form of equation (3.16) may be written as:

$$\mu_m = \sum_{i=1}^{n} \frac{\mu_i}{1+\frac{1}{x_i}\sum_{j=1,j\neq i}^{j=n} x_i\,\emptyset_{ij}} \quad (3.17)$$

$$\emptyset_{ij} = \frac{\left[1+\left(\frac{\mu_i}{\mu_j}\right)^{\frac{1}{2}}\left(\frac{M_j}{M_i}\right)^{\frac{1}{4}}\right]^2}{(2\sqrt{2})\times\left[1+\left(\frac{M_i}{M_j}\right)\right]^{\frac{1}{2}}} \quad (3.18)$$

where,

μ_m = viscosity of the mixture.

μ = viscosity, g/cm-sec.; μ_1, μ_2, etc. refer to the pure components at the

temperature and pressure of the mixture.

x_1, x_2, = mole fraction of a components in a mixture.

Φ_{ij} = dimensionless constant.

M = molecular weight.

Following data has been recorded during experiments, and some of them are calculated by using empirical equations. Further, these input parameters are used in Leith and Licht model for calculating the pressure drop and collection efficiency.

- **For feedstock – Wood;**

Inlet flow rate (V_0)	= 0.014	Viscosity (μ)	= 1.84×10^{-05}
Temperature (T)	= 320	Density of gas (ρ_g)	= 1.325
Particles density (ρ_p)	= 2200		

- **For feedstock – Wood with 10 wt.% CaO;**

Inlet flow rate (V_0)	= 0.016	Viscosity (μ)	= 1.56×10^{-05}
Temperature (T)	= 313.4	Density of gas (ρ_g)	= 1.5
Particles density (ρ_p)	= 2200		

- **For feedstock – Coconut shell;**

Inlet flow rate (V_0)	= 0.013	Viscosity (μ)	= 1.67×10^{-05}
Temperature (T)	= 314	Density of gas (ρ_g)	= 1.45
Particles density (ρ_p)	= 2200		

- **For feedstock – Coconut shell with 10 wt.% CaO;**

Inlet flow rate (V_0)	= 0.0098	Viscosity (μ)	= 1.72×10^{-05}
Temperature (T)	= 312	Density of gas (ρ_g)	= 1.4
Particles density (ρ_p)	= 2200		

Table 3.4 shows the particle size efficiency for the different diameters of dust particles present in the producer gas. The producer gas is obtained from biomass feedstock wood and coconut shell. In case-1, these feedstocks are used one by one alone. In case -2, these feedstocks are mixed with 10 wt% CaO and used one by one alone.

Table 3.4: Particle size efficiency for different feedstocks. (Empirically using Leith and Licht model).

Particle diameter (m)	Efficiency (η) %, Wood	Efficiency (η) %, Wood + 10 wt.% CaO.	Efficiency (η) %, Coconut shell	Efficiency (η) %, Coconut shell + 10 wt.% CaO.
$1.00x10^{-06}$	0.353368	0.475488	0.361132	0.266783
$2.00x10^{-06}$	1.405998	1.888429	1.436723	1.06287
$5.00x10^{-06}$	8.46955	11.23302	8.647679	6.460364
$10.00x10^{-06}$	29.81208	37.91227	30.35686	23.44339
$15.00x10^{-06}$	54.90895	65.78135	55.6926	45.17722
$20.00x10^{-06}$	75.73113	85.13986	76.47588	65.64968
$30.00x10^{-06}$	95.86608	98.62895	96.14606	90.96674
$40.00x10^{-06}$	99.6531	99.95124	99.69377	98.60773
$50.00x10^{-06}$	99.98566	99.99933	99.9882	99.87423
Pressure drop	152.16	225.75	144.06	80.50

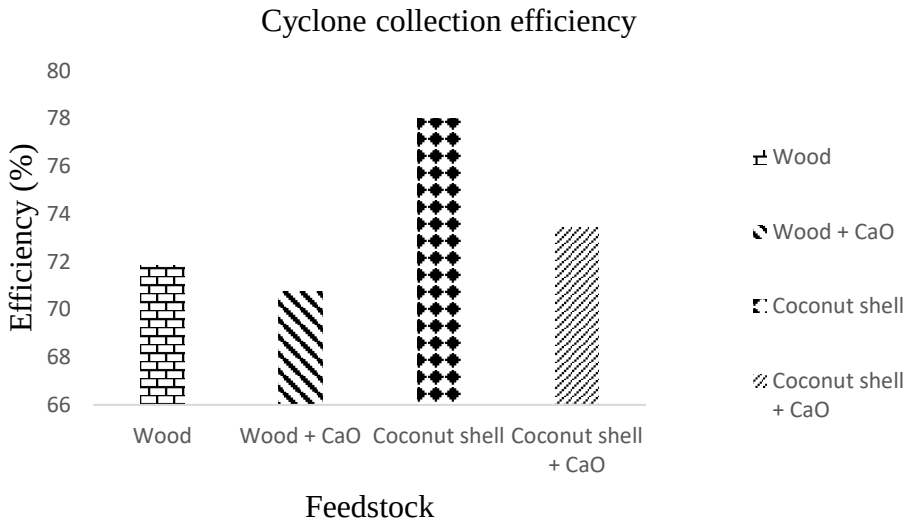

Figure 3.10: Shows the cyclone collection efficiency for different feedstocks (Experimental).

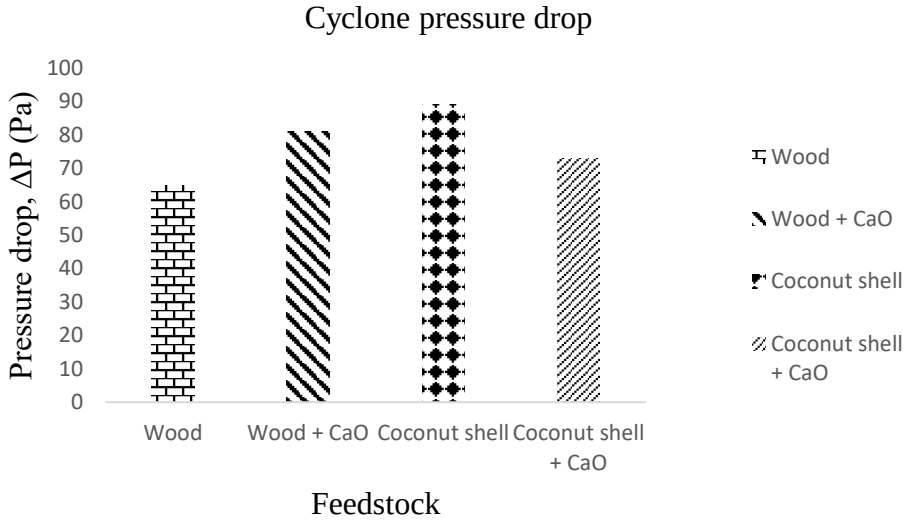

Figure 3.11: Shows the variation of cyclone pressure drop Vs different feedstock used for gasification.

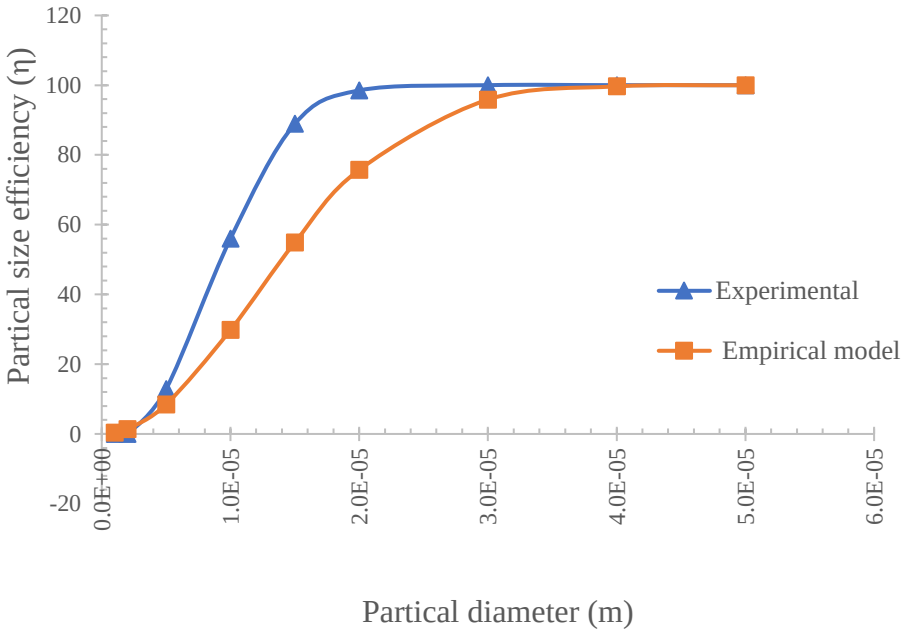

Figure 3.12: Shows the comparison of particle size efficiency between experimental and empirical model when producer gas is obtained from the wood feedstock.

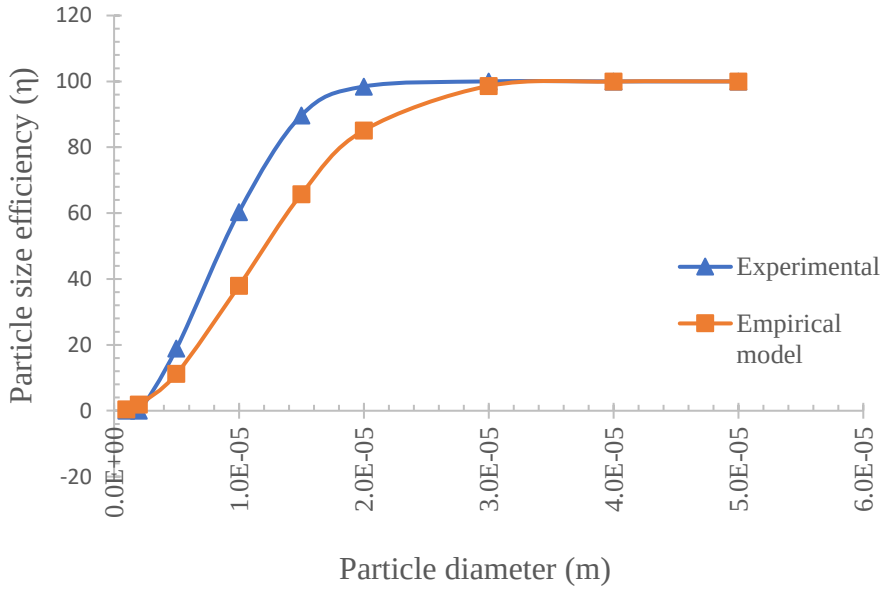

Figure 3.13: Shows the comparison of particle size efficiency between experimental and empirical model when producer gas is obtained from the wood + 10 wt. % *CaO* feedstock.

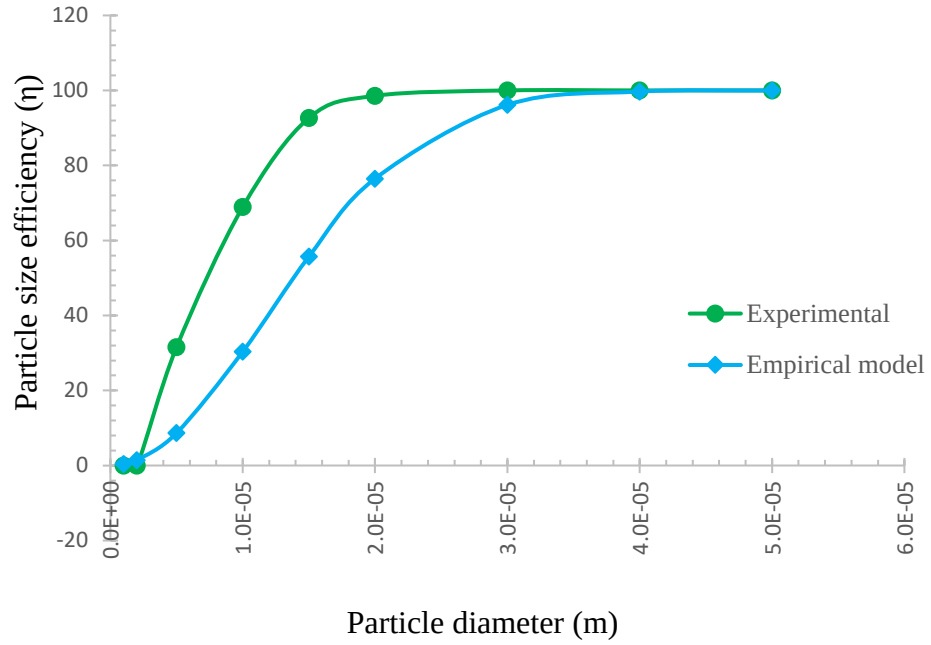

Figure 3.14: Shows the comparison of particle size efficiency between experimental and empirical model when producer gas is obtained from the coconut shell feedstock.

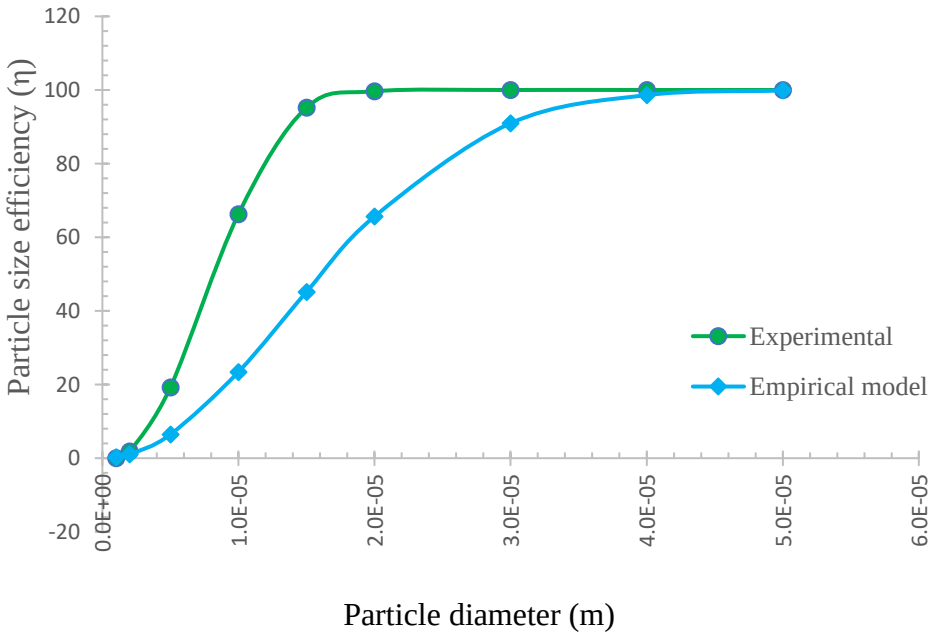

Figure 3.15: Shows the comparison of particle size efficiency between experimental and empirical model when producer gas is obtained from the coconut shell + 10 wt. % *CaO* feedstock.

Figure 3.10 shows the cyclone collection efficiency obtained for different feedstock by experimental method. It is clear from the figure that the cyclone collection efficiency for coconut shell is higher than other feedstocks used. This is due to the difference in density and viscosity of producer gas for each feedstock, and these differences affect the flow rate of producer gas into the system. On the other hand, using *CaO* with feedstock, the efficiency decreases due to the reduction in inlet loading and heavy particles.

Figure 3.11 shows the variation in cyclone pressure drop with different feedstocks to be used for gasification. It is clear from the figure that the pressure drop varies with inlet flow rate and cyclone dimensions. Keeping dimensions constant, flow rate varies due to quality of gas, as a result, variation in pressure drop is seen.

In figure 3.12, we show the comparison of dust particle size efficiency between the experimental model and predicted empirical model when producer gas is obtained from the wood feedstock. Viewing the figure, it is clear that the experimental data is very close to the values calculated by the empirical model. This closeness in results demonstrates the accuracy of the experimental data.

Figure 3.13 shows the effect of calcium oxide on dust particles when mixed with wood feedstock for gasification. Mixing of 10 *wt. % CaO* with feedstock decreases the particle size efficiency because when feedstock burns inside the combustion chamber, the *CaO* reacts with the gas and settle down the heavy particles. The particle size affects the performance of the system. It means the lighter particle accounts for higher efficiency in both cases, experimental and Leith and Licht model.

In figure 3.14 and 3.15, coconut shell with and without 10 *wt. % CaO* is used for gasification. The graph trend for dust particle size for coconut shell is very similar to that of wood feedstock when compared between the experimental and empirical model.

Although, producer gas is an excellent alternative fuel for the existing dual-fuelled diesel engine when used together with conventional diesel. The quality of the producer gas is not constant all the time because of the impurities present in the producer gas and hence, the diesel consumption varies in accordance with the producer gas quality. So, to compensate the diesel consumption, the blending of biodiesel with conventional diesel comes into the play and therefore, depth analysis of biodiesel is needed on its emissions, calorific value and storage time.

3.5 Biodiesel

The use of plant oil is the possible alternative fuel like vegetable oils and tree-borne seeds. These alternative diesel fuels are known as biodiesel having low emission, non-toxic when it is compared with the conventional diesel. The utilisation of biodiesel will help to make the proper balance between the environment, agriculture and economic point of view. Oils/fats chemically comprise long-chain of fatty acids having three molecules of triglyceride that are ester bonded to a single glycerol molecule. These fatty acids are differed by the carbon chains length, its number, location and double bonds position in the carbon chain. Thus, biodiesel is to be considered as lower alkyl esters of long-chain fatty acids which are prepared either by esterification of fatty acids or by transesterification with lower alcohols [11].

Advantages: Biodiesel needs no modification in the existing engines. It is purely made for the vegetable sources and does not contain any aromatic hydrocarbons, sulfur, metals or crude oil residues. Biodiesel is an oxygenated fuel; the quantity of soot and carbon monoxide is less with comparison to the conventional diesel. Using biodiesel as a fuel does not entirely responsible for global warming as CO_2 emitted is absorbed by the plants for its growth, and therefore, CO_2 is maintained [12].

Disadvantages: The production cost of biodiesel is higher than the conventional diesel fuel. Biodiesel is mainly produced from the edible oil, which affects food availability and thereby prices increases. Use of biodiesel is not favourable in low temperature; also, it is only used in diesel engines. Moisture attack more likely than conventional diesel. The concentration of *NOx* found more in its emission [13].

3.5.1 Biodiesel production procedures:

Various processes are adopted to use the biodiesel as a fuel either by blend with conventional diesel or using as monoalkyl ester formed after getting various chemical reaction processes. Different methods of biodiesel manufacturing are; Direct use and blending, Microemulsification, Thermal cracking (pyrolysis), Transesterification (Alcoholysis).

In view of the all manufacturing methods, we are interested in adopting the transesterification process for biodiesel production out of all [14].

- **Transesterification (Alcoholysis):**

  Conversion of fat or oil with the help of alcohol to obtained easter and glycerol by a chemical reaction is known as transesterification or alcoholysis. During the process of getting easter and glycerol, a catalyst is used to increase the reaction rate as well as yield. As the reaction is reversible, more amount of alcohol is used to transform the equilibrium position to the product side. Alkalis, acids, or enzymes can catalyse the reaction. These alkalis included *KOH, NaOH*, carbonates and their corresponding's sodium and potassium alkoxides like-sodium methoxide, sodium ethoxide, sodium propoxide and sodium butoxide. For an acid catalyst, Sulfuric acid, sulfonic acids and hydrochloric acid are generally used whereas Lipases can be used as biocatalysts. After using these catalysts, it is found that the reaction rate of Alkali-catalysed transesterification is much more

faster the acid-catalysed transesterification, therefore, alkali- catalyst is usually used for commercial purpose. Although, using alkali-catalysed transesterification reaction, triglycerides required Low free fatty acid content as well as more water. For cleaning the triglycerides, saponification can be done [14]. Transesterification process is widely used for reducing the high viscosity of triglycerides

As the transesterification is a reversible reaction, the mixing of reactant is essential to proceed the reaction. However, the presence of a catalyst (strong acid or base) in the reaction increases the conversion rate. Equation (3.19) represents the transesterification reaction [11]. Dense, liquid phase rich in glycerol is the by-product of this process and the fatty esters have cetane number and heating value closer to diesel [15].

$$\underset{\text{Ester}}{RCOOR^1} + \underset{\text{Alcohol}}{R^2OH} \overset{\text{Catalyst}}{\rightleftharpoons} \underset{\text{Ester}}{RCOOR^2} + \underset{\text{Alcohol}}{R^1OH} \tag{3.19}$$

Using methanol in this process is called methanolysis. Equation (3.20) represents the methanolysis of triglyceride.

$$\underset{\text{Triglyceride}}{\begin{matrix} CH_2-OCOR^1 \\ | \\ CH-OCOR^2 \\ | \\ CH_2-OCOR^3 \end{matrix}} + \underset{\text{Methanol}}{3CH_3OH} \rightleftharpoons \underset{\text{Glycerol}}{\begin{matrix} CH_2OH \\ | \\ CHOH \\ | \\ CH_2OH \end{matrix}} + \underset{\text{Methyl esters}}{\begin{matrix} R^1COOCH_3 \\ R^2COOCH_3 \\ R^3COOCH_3 \end{matrix}} \tag{3.20}$$

3.5.2 Storage of biodiesel:

During the oxidation of vegetable oils and their esters (biodiesel), they degenerate very quickly than conventional diesel. The presence of unsaturated fatty acids in vegetable oil is susceptible to oxidation. Although exposure to ambient air, sunlight, contact with metals and high-temperature conditions increases the oxidation reactions, thereby

reducing the oxidation stability of biodiesel [16]. The quality of biodiesel is governed by various flow characteristics like- kinematic viscosity, peroxide value, acid value, oxidation stability index etc. Whereas burning characteristics can be regulated by heating value, brake specific fuel consumptions, emissions etc. these all alter with storage time.

3.5.3 Quality measuring parameters:

Following parameters are used to measure the quality of the biodiesel, which mentioned below.

a) Kinematic viscosity;

Viscosity is the flow measuring parameter of a fluid which indicates the resistance to the gradual deformation by shear stress or tensile stress. In simple words, viscosity is the resistance to flow of a fluid. Its SI unit is Nsm^{-2}. Kinematic viscosity is given by:-

$$\text{Kinematic viscosity} = \frac{\text{Dynamic viscosity of the fluid}}{\text{density of the fluid}} \tag{3.21}$$

Its SI unit is m^2s^{-1}. The kinematic viscosity of a biodiesel is generally measured in mm^2s^{-1}. For biodiesel, the kinematic viscosity must lie between 1.9 - 6.0 mm^2s^{-1}at 313 *K*, in accordance with *ASTM* 6751-11b [17].

b) Brake specific fuel consumption;

The ratio of the mass of fuel consumption to the brake effective power is known as Brake-specific fuel consumption (BSFC). For a particular fuel, thermal efficiency is inversely proportional to the *BSFC*. Equation (3.22) represents the *BSFC* [12].

$$\text{BSFC} = \frac{\text{mass ofthe fuel consumed}}{\text{effective brake power}} = \frac{1}{\text{thermal efficiency}} \tag{3.22}$$

c) Emissions:

Emissions of a fuel when combusted mainly consists of hydrocarbons, carbon monoxide, oxides of nitrogen, sulphur oxides and particulates. Amount of unburnt hydrocarbons (UBHC) decreases with the replacement of commercial diesel oil with biodiesel. There is a minimal decrease in the carbon monoxide amount in the emissions while oxides of nitrogen have an enhanced amount in the emissions in comparison to burning of conventional diesel [17].

Photograph of biodiesel production unit by transesterification method.

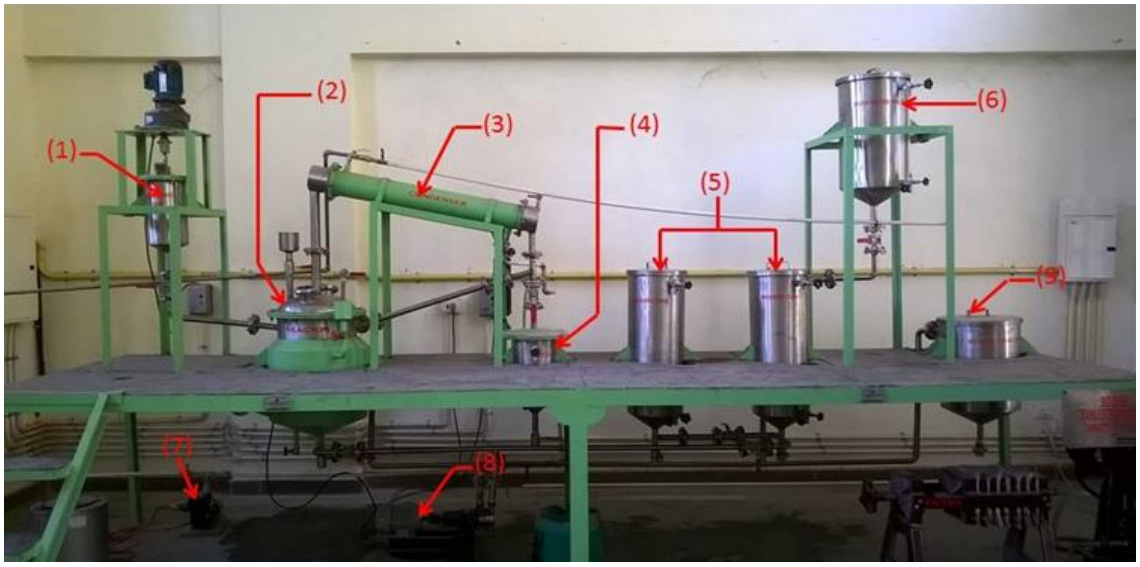

Figure 3.16: Experimental setup of biodiesel production unit by transesterification method installed in IIT (BHU). 1) Caustic mixing tank, 2) Reactor, 3) Condenser, 4) Receiver, 5) Washing tank, 6) Wash water holder, 7) Centrifugal pump, 8) Reciprocating pump, 9) Storage tank.

3.5.4 Instrumentation:

While conducting the experiment, various apparatus was used to measure the input and output values of the setup. These equipment's are as follows:

a) Capillary flow viscometer:

Capillary flow viscometer is used to measure the viscosity of the sample oil or any other liquid.

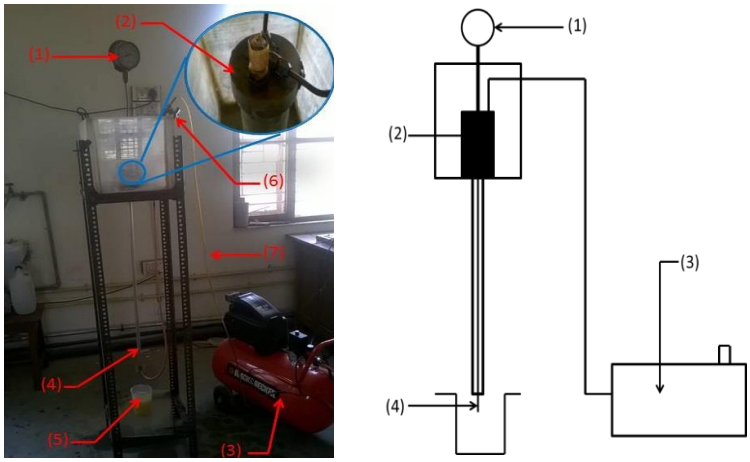

(a) (b)

Figure 3.17: (a) Experimental setup for capillary flow viscometer installed in IIT (BHU), (b) Schematic representation. 1) Pressure gauge, 2) Receiver, 3) Air compressor unit, 4) Capillary tube, 5) Collecting beaker, 6) Pressure regulator, 7) Inlet pipe.

Capillary flow viscometer works on the principle that when a fluid flows through a tube or on any surface, it experiences shear stress at the boundary which hinders the flow of the fluid. Pressure gauge (1) is used to measure the pressure of air inside the reservoir. It carries the unit's pounds per square inch (psi) and kilogram per square centimetres (kg/cm^2). Reservoir (2) stores in the sample fluid. Its internal diameter is 3.5 inches. It contains a knob which is closed before the pressure inside the reservoir is made above the atmospheric pressure. It contains an opening at its roof for the pressurized air to enter. The increase in the air pressure is measured from (1). Capillary tube (4) is used to measure the shear stress at the inner wall and fluid interface. The fluid flows through the capillary at various pressure differences. The length of the tube is one metre and its internal diameter is 2 millimetres. The flown liquid is collected in the collecting beaker (5).

Air compressor unit (3) is used to develop pressurized air and is sent into the reservoir. The pressure regulator (6) is used to alter the pressure of air inside the reservoir.

b) Bomb calorimeter:

A bomb calorimeter is a type of constant-volume calorimeter used in measuring the heat of combustion of a particular reaction. Other details are already mentioned in the previous section, 2.4.2.4. Block diagram is used to present its working.

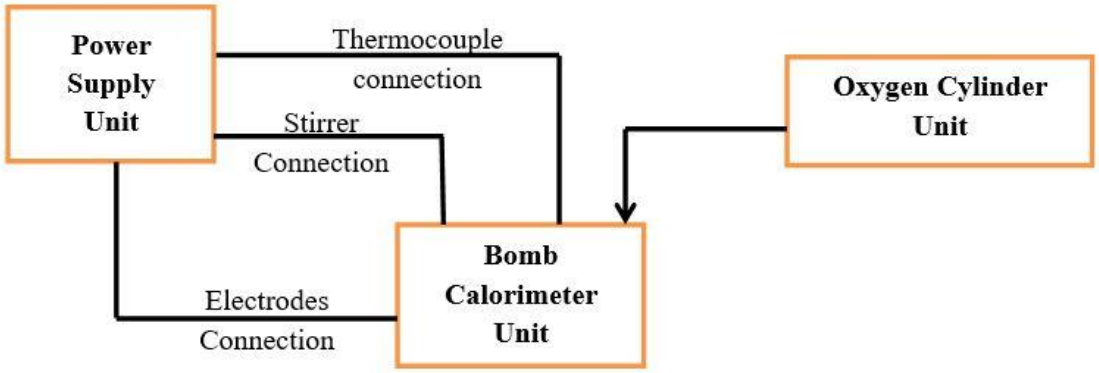

Figure 3.18: Block diagram representation of experimental setup of bomb calorimeter.

c) Variable compression ratio (VCR) engine research test setup:

Photograph of variable compression ratio (VCR) engine.

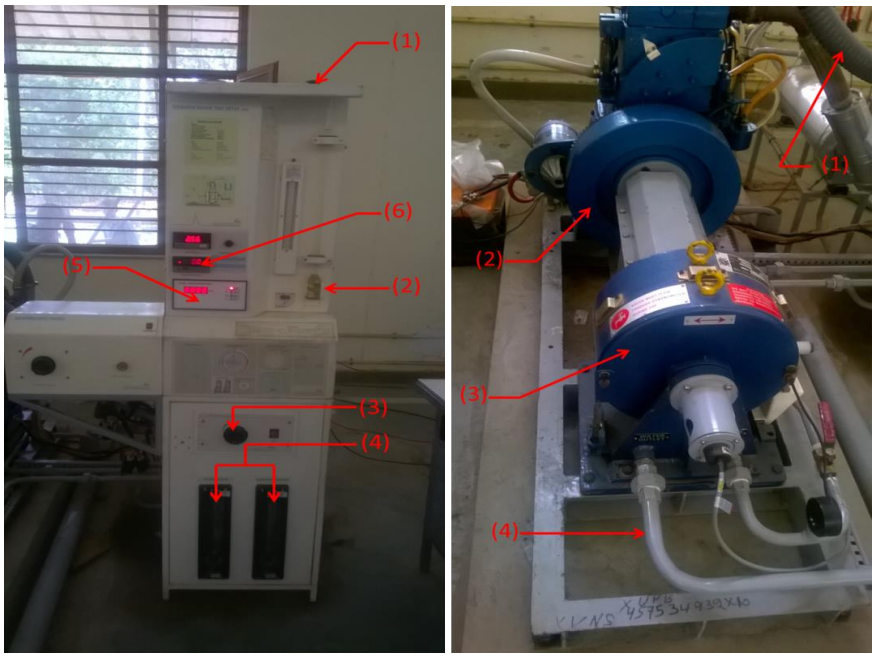

(a) (b)

Figure 3.19: Experimental setup of variable compression ratio engine installed in IIT (BHU). (a) # 1) Reservoir, 2) Oil level, 3) Load application knob, 4) Rotameter, 5) Speed, 6) Load indicator. (b) # 1) Exhaust pipe, 2) Flywheel housing, 3) Dynamometer, 4) Water pipe.

3.6 Biodiesel production procedure

The biodiesel used for the experiment is produced from the parent oil through the process of transesterification. The reactants used for the process include the parent oil, sodium hydroxide or potassium hydroxide (to be used as a catalyst) and alcohol. The block diagram representation of the biodiesel production procedure is given below: -

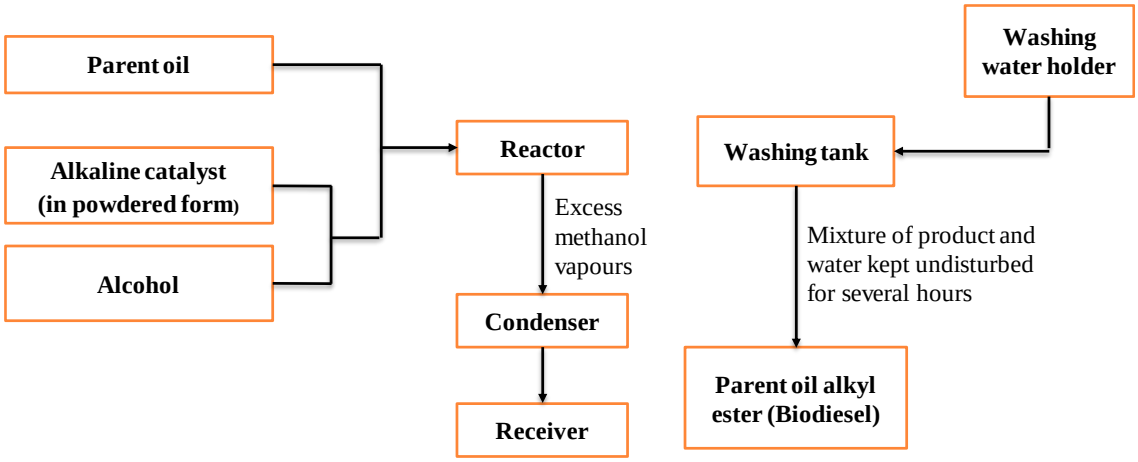

Figure 3.20: Block diagram representation of biodiesel transesterification unit.

The parent oil is mixed with the reactants (alkaline catalyst and alcohol) in the reactor unit. The reaction of esterification takes place at a particular temperature with the help of a heating element present at the base of the reactor. The reaction time depends upon the nature of the parent oil. The excess amount of alcohol gets vaporised and enters into the condenser unit where it is condensed and collected in the receiver tank. After the completion of the reaction, the mixture (parent oil alkyl ester and glycerol), is transferred to the washing tank with the help of a reciprocating pump. After the transfer of the mixture, water is added to it from the water holder, and the mixture is now left undisturbed for nearly 24 hours. After 24 hours, the water and glycerol separate from the alkyl esters due to the density difference of different components and therefore, the alkyl ester is separated from the mixture.

The experiment of biodiesel production was carried out by using soyabean oil as the parent oil, sodium hydroxide as the catalyst and methanol as the corresponding alcoholic reactant. Table 3.5 indicates the various reactants used in the experiments and the corresponding reaction conditions and outputs.

Table 3.5: Experimental conditions and output parameters.

Serial No.	Reactants/Parameters/Outputs	Values/Name
1.	Parent oil – volume	Soyabean Oil – 5 litres
2.	Alcohol – volume	Methanol - 833ml
3.	Alcohol : oil ratio	1:6
4.	Catalyst – amount	NaOH –1% (w/v) of oil
5.	Reaction temperature	75-80^{o}C
6.	Reaction time	1 hour 30 minutes
7.	Settling time	28 hours
8.	Biodiesel output	3.45 litres
9.	Density of biodiesel	866 kgm^{-3}

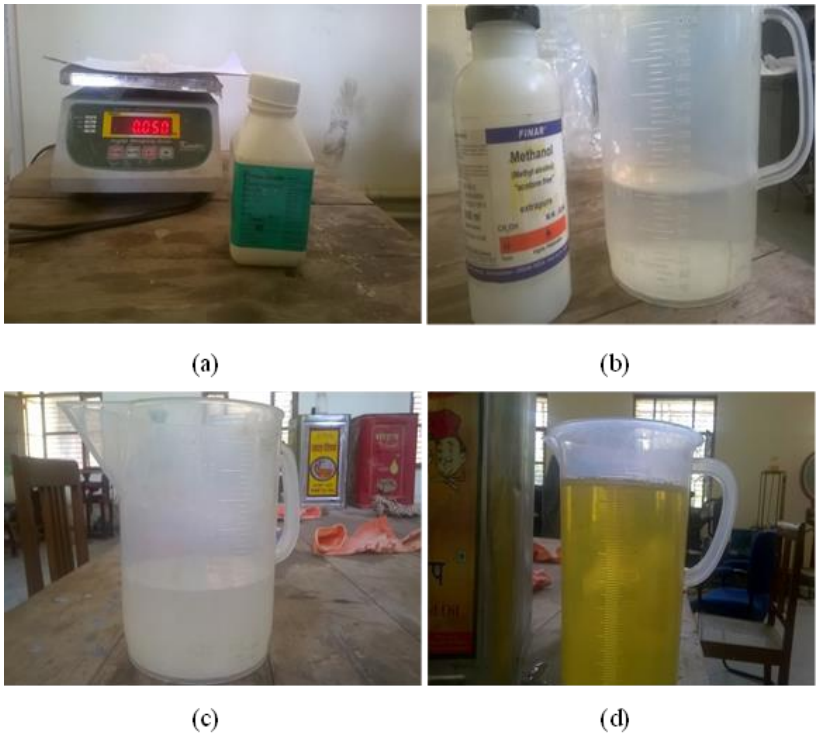

Figure 3.21: Soyabean methyl ester preparation, (a) Catalyst *NaOH* in 1% *(w/v)* of oil i.e. 50 grams. (b) Reactant methanol in 1:6 alcohol to oil ratio i.e. 833 *ml*. (c) Mixture of *NaOH* and methanol obtained by continuous stirring. (d) Soyabean oil.

(e) (f)

Figure 3.22: Soyabean methyl ester preparation, (e) Pouring of reactants and catalyst into the reactor. (f) Reaction temperature maintained at 75^{o}C - 80^{o}C with the help of a heating element.

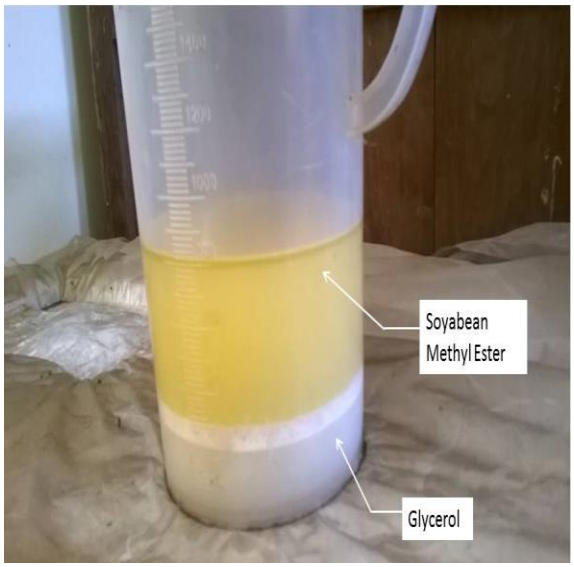

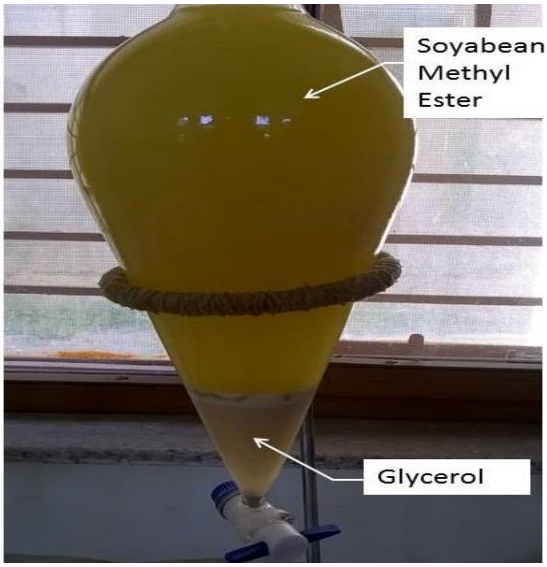

(g) (h)

Figure 3.23: Soyabean methyl ester preparation, (g) & (h) Separation of glycerol from Soyabean methyl ester after 28 hours of undisturbed condition.

3.6.1 Viscosity of biodiesel:

- **Procedure:**

  Dynamic viscosity of the biodiesel prepared is measured from the "Capillary flow viscometer".

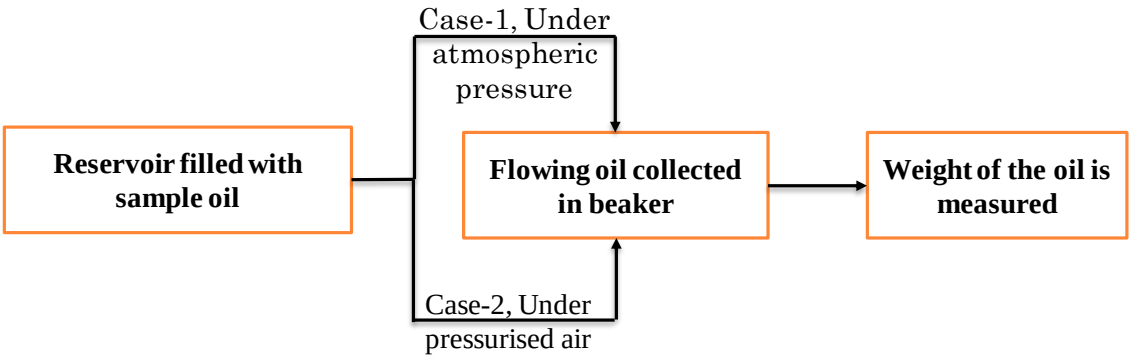

Figure 3.24: Block diagram representation of experimental procedure for measuring viscosity.

For the measurement of the viscosity of the sample oil, firstly the reservoir was filled with the sample oil through an opening provided at the top of the reservoir. The height of the oil in the reservoir was measured which indicated the initial height of the oil in the reservoir *(Y_1)*. A beaker was placed at the bottom just below the capillary tube and the stop cock was removed. With the help of a stopwatch and a digital weight measuring instrument, the weight of oil collected in the beaker in a stipulated time period (which remains constant for the entire reading) was measured. The initial reading was taken at the atmospheric pressure by opening the inlet section situated at the top of the reservoir and the subsequent readings were taken at a higher pressure range from 0.2 kg/cm^2 to maximum possible. These reading were taken about 6 to 7 times. After the completion of the measurement, again the height of the oil left in the reservoir was measured.

- **Calculations:**

  Governing equation: -

$$\tau_{\omega} = -K\left(\frac{du}{dy}\right)^{n} \quad (3.23)$$

where,

τ_{ω} = shear stress at wall, Nm^{-2}

K = Consistency constant or proportionality constant = μ/g.

μ = Dynamic viscosity of the fluid.

n = Flow behaviour index

$\frac{du}{dy}$ = shear rate or rate of deformation = $\frac{8U}{d}$ for fully developed laminar and turbulent flow.

U = Average velocity of the fluid and *d* is the internal diameter of the capillary tube *(d = 2mm).*

Taking $\log_{10}$ on LHS and RHS, we get,

$$\log_{10}\tau_{\omega} = \log_{10}K + n\log_{10}\left(\frac{du}{dy}\right) \quad (3.24)$$

which represents the equation of a straight line, of the form *Y=mX+C* where m is the slope of the straight line.

$$U = \frac{\Delta W/t}{\rho(\pi d^2/4)} \quad (3.25)$$

where,

ΔW = weight of the liquid collected in time t seconds, kg

ρ = density of the liquid, kgm^{-3}

d = diameter of capillary tube = 2mm

From equation (3.25) and shear rate relation with *U*, the shear rate can be calculated putting the value of *d* as 2 mm.

Differential pressure at the point of collecting fluid will be: -

$$\Delta P = (h_f + L_c)\rho g + P_g \tag{3.26}$$

where,

h_f = height of the liquid in the main reservoir with internal diameter of 3.5 cm × 2.54 cm.

L_c = length of the capillary tube = 1m

P_g= Gauge pressure, Nm^{-2}

$$\tau_w = \frac{d\Delta P}{4L_c} \tag{3.27}$$

From equations (3.26) and (3.27), the shear stress at the wall can be calculated.

For values of h_f, Y_1 represents the initial height of the fluid in the reservoir and the values of Y_2, Y_3, Y_4, etc. are given by: -

$Y_2 = Y_1 - (4\Delta W_1/\rho\pi D^2)$

$Y_3 = Y_2 - (4\Delta W_2/\rho\pi D^2)$ and so on ;

where,

D= internal diameter of the reservoir.

Graph is drawn between shear stress and shear rate on a log-log scale and the slope of the mean straight line obtained from the experimental and further calculated values gives the flow index.

$$\mu = \frac{g\tau_\omega}{\left(\frac{du}{dy}\right)^n} \tag{3.28}$$

where,

μ = dynamic viscosity, Nsm^{-2}

From equation (3.28), the viscosity of the fluid can be calculated and by dividing this value with its density, its kinematic viscosity can be calculated and its unit will be m^2s^{-1}.

- **Experiment:**

  The experiment was carried out with the soybean methyl ester (biodiesel) with a time interval of 2 days. Table 3.6 depicts the calculation of the initial reading of viscosity of the biodiesel, and the same procedure followed for the subsequent readings. Figure 3.25, represents the graph between the logarithm of shear stress and shear rate and the slope of which would give the flow index and the corresponding dynamic viscosity of the fluid.

Table 3.6: Calculation for initial reading of viscosity of *SBME* (biodiesel).

Serial No.	h_f, (m)	P_g, (kg/cm^2)	ΔP, (N/m^2)	τ_{ω}, (N/m^2)	Shear rate = du/dy, (s^{-1})
1.	0.096	0	9891.62	4.946	415.2
2.	0.0955	0.2	11265.82	5.633	3736.8
3.	0.0907	0.3	11912.61	5.956	4013.6
4.	0.0856	0.4	12556.27	6.278	4567.2
5.	0.0798	0.5	13193.60	6.597	4844
6.	0.0737	0.6	13827.77	6.914	5536

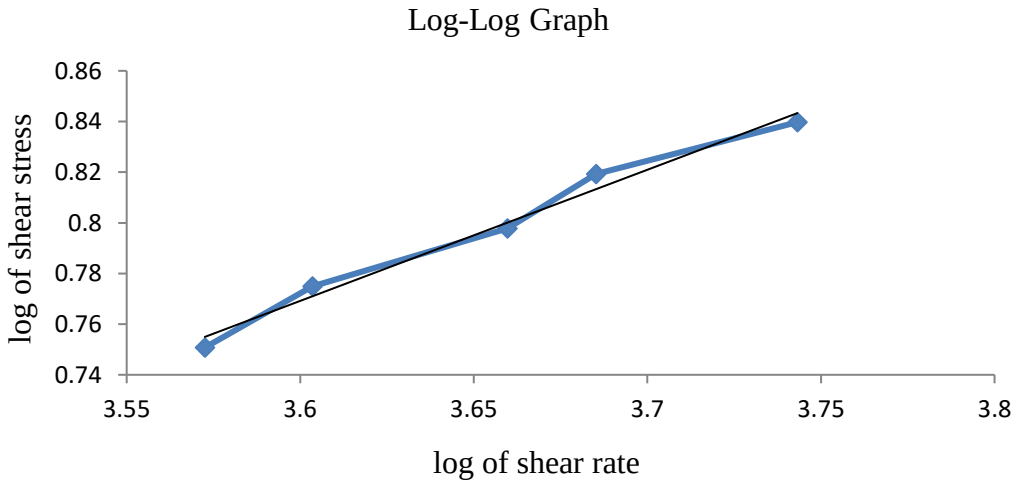

Figure 3.25: Graph between log of shear stress and log of shear rate.

The slope of the mean line was found out to be 1.53, and the corresponding dynamic viscosity and kinematic viscosity *(ν)* were 3.957×10^{-3} *Pa s* and 4.57 mm^2/s.

Table 3.7: Viscosity measured for different storage time of *SBME* (biodiesel).

S. No.	Day	Room temperature, (^oC)	Dynamic viscosity (μ), (Pa s)	Kinematic viscosity (ν), (mm^2/s)
01.	0	36.8	$3.957 \text{ X } 10^{-3}$	4.57
02.	4	34.5	0.03428	39.5
03.	8	34.8	0.04049	46.76
04.	10	34.4	0.04164	48.08
05.	14	35.1	0.08774	101.33

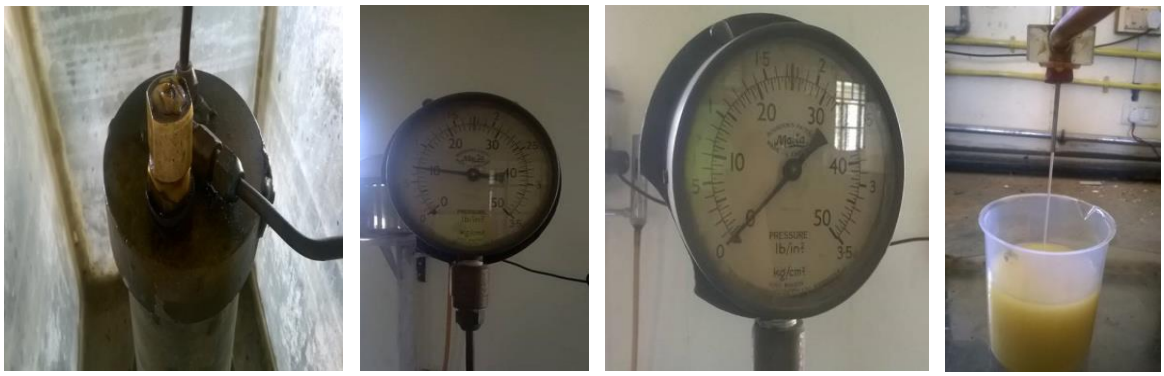

(a) (b) (c) (d)

Figure 3.26: Viscosity measuring process, (a) Reservoir containing the Soyabean biodiesel, (b) Pressure greater than atmospheric pressure (c) Atmospheric pressure, (d) SBME collection in beaker at different pressure in a stipulated time period.

3.6.2 Calorific value of biodiesel:

The calorific value of the sample oil is measured by using bomb calorimeter. The detailed discussion has already mentioned in the previous section, 2.4.2.4. Also, to explain the experiment, the block diagram is used to present the complete process.

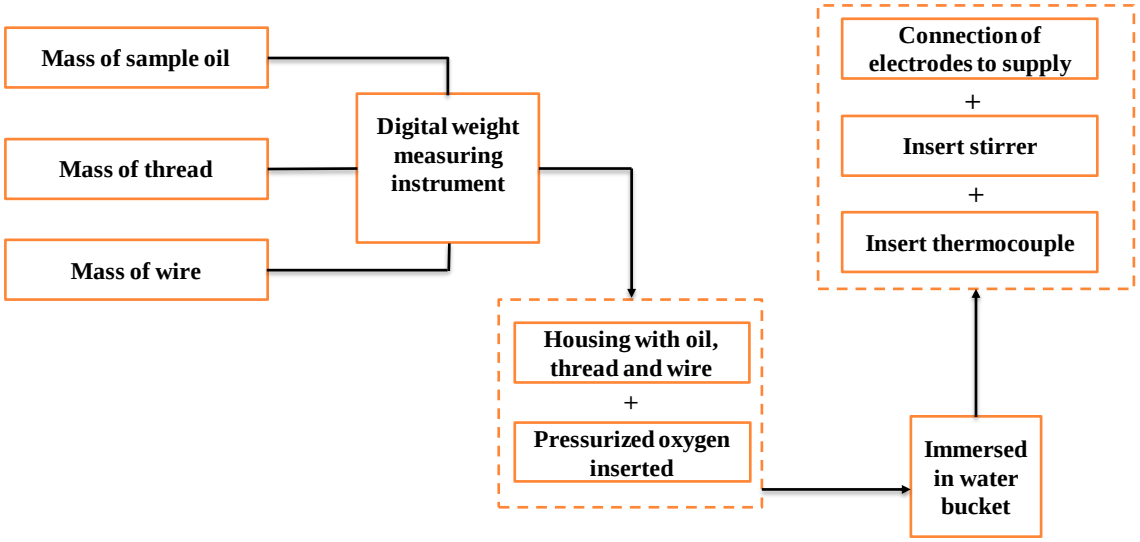

Figure 3.27: Block diagram representation of experimental procedure for measuring calorific value from bomb calorimeter.

- **Calculation:**

$$m_f(CV)_f + m_{th}(CV)_{th} + m_w(CV)_w = m_{water}C_p\Delta T \quad (3.29)$$

where,

m_f = mass of the fuel, in kg

$(CV)_f$ = calorific value of fuel, in kcal/kg

m_{th} = mass of the thread, in mg

$(CV)_{th}$ = calorific value of thread = 4.18 kcal/mg

m_w = mass of wire, in mg

$(CV)_w$ = calorific value of wire = 0.335 kcal/mg

m_{water} = mass of water, in kg

C_p = specific heat at constant pressure of water = 1.005 kcal/kg

Equation (3.29) used for measuring the calorific value of Soyabean methyl ester (biodiesel). Table 3.8 depicts the various experimental input measurements for the determination of the calorific value of the biodiesel before storage, i.e. at day 0.

Table 3.8: Determination of calorific value of fresh Soyabean methyl ester (biodiesel).

Inputs	Values
Mass of fuel (m_f)	1.2792 g
Mass of wire (m_w)	15.4 mg
Mass of thread (m_{th})	19.4 mg
Mass of water (m_{water})	2 kg
Rise in temperature (ΔT)	4.78 ^oC
Calorific value	30.957 MJ/kg

The same process applied to measure the calorific value of *SBME* (biodiesel) at different storage time. These calorific values are shown in Table 3.9.

Table 3.9: Calorific value of pure biodiesel at varying storage time interval.

Serial no.	Day	Calorific value, (MJ/kg)
1.	0	30.957
2.	4	29.140
3.	8	30.977
4.	10	30.886
5.	14	30.520

3.6.3 Variable compression ratio (VCR) research test setup:

- **Procedure:**

  For the measurement of the emissions, the engine runs at three blends ratio, B10 (10% Biodiesel + 90% Diesel), B20 (20% Biodiesel + 80% Diesel) and B30 (30% Biodiesel + 70% Diesel) at different loads (0, 2, 4, 6, 8, 10, 12 kgs) with various

compression ratio (15:1, 16:1, 17:1 and 18:1). The density and calorific value of the respective blended fuels are calculated before commencement of the experiment. Now at different compression ratio and load, the emissions were noted and graphs plotted for particular emission composition between compression ratio and load. Figure 3.28 gives the schematic representation of the experimental procedure.

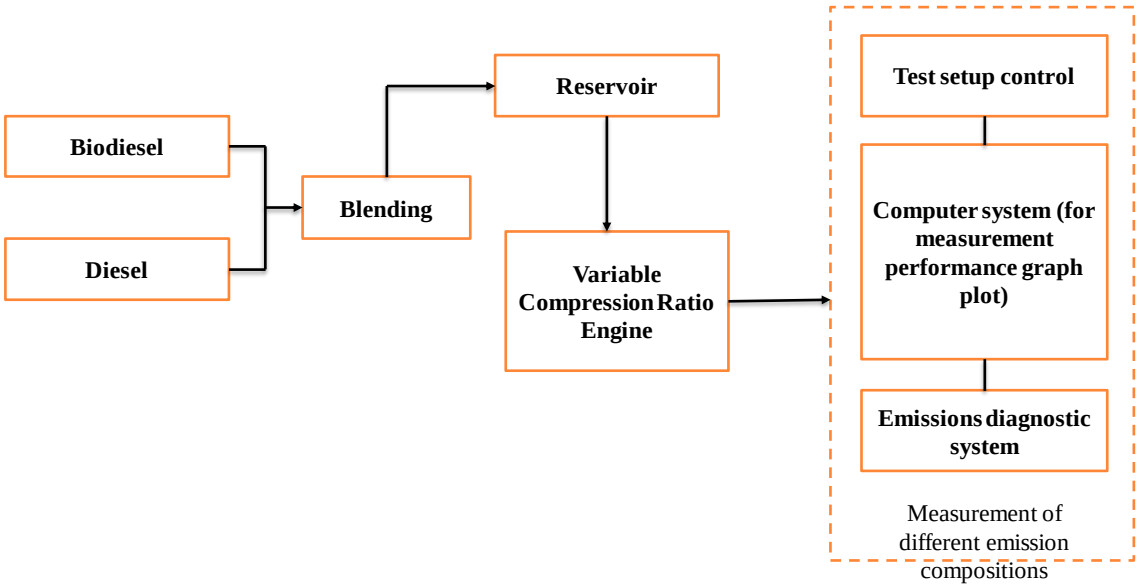

Figure 3.28: Block diagram representation of experimental procedure to measure the emissions of B10, B20 and B30 biodiesel blends with various loads and compression ratios.

3.7 Experiment

The experiment was conducted at *B10, B20* and *B30 SBME* (biodiesel) blends with diesel oil for 18:1, 17:1, 16:1and 15:1 compression ratio at 0, 2, 4, 6, 8, 10 and 12 *kg* loads and corresponding emissions-CO, HC, NO, CO_2, and O_2 were recorded sequentially. Table 3.10 to 3.12, show the different emissions at different compression ratios and loads for *B10, B20* and *B30 SBME* (biodiesel) blend with diesel oil respectively.

Table 3.10: Emissions at various loads and compression ratios for *B10* blend of *SBME* (biodiesel) with diesel oil.

Compression ratio	Load (kg)	CO (%vol)	HC (ppm)	NO (ppm)	CO_2 (%vol)	O_2 (%vol)
18:1	0	0.08	53	72	1.45	18.43
	2	0.05	50	257	2.18	17.36
	4	0.04	48	348	2.38	17.18
	6	0.05	50	407	2.46	17.01
	8	0.03	49	400	2.27	17.36
	10	0.03	48	380	2.1	17.59
	12	0.03	46	294	1.84	17.98
17:1	0	0.15	84	38	1.58	18.04
	2	0.09	78	245	2.51	16.7
	4	0.06	80	337	2.68	16.53
	6	0.06	82	398	2.68	16.45
	8	0.05	81	374	2.49	16.75
	10	0.04	76	331	2.16	17.25
	12	0.04	68	271	1.9	17.67
16:1	0	0.13	87	36	1.35	18.42
	2	0.1	92	167	2.25	17.15
	4	0.09	96	242	2.42	16.9
	6	0.07	99	271	2.38	17.15
	8	0.06	100	292	2.25	17.28
	10	0.05	100	228	1.91	17.82
	12	0.06	102	186	1.71	18.22
15:1	0	0.23	206	25	1.66	18.49
	2	0.2	216	130	2.62	17.26
	4	0.19	226	203	2.85	17.08
	6	0.17	239	245	2.83	17.18
	8	0.16	242	243	2.74	17.45
	10	0.16	242	212	2.48	17.85
	12	0.17	240	179	2.17	18.35

Table 3.11: Emissions at various loads and compression ratios for *B20* blend of *SBME* (biodiesel) with diesel oil.

Compression ratio	Load (kg)	CO (%vol)	HC (ppm)	NO (ppm)	CO_2 (%vol)	O_2 (%vol)
18:1	0	0.08	60	113	1.74	18.04
	2	0.06	68	350	2.72	16.61
	4	0.06	83	408	2.89	16.53
	6	0.06	91	455	2.81	16.64
	8	0.06	95	450	2.62	16.99
	10	0.05	93	350	2.2	17.62
	12	0.04	75	280	1.76	18.22
17:1	0	0.15	98	58	1.66	18.47
	2	0.16	180	245	2.88	16.89
	4	0.18	221	324	3.14	16.64
	6	0.2	245	386	3.4	16.36
	8	0.19	258	436	3.48	16.39
	10	0.19	268	330	3.01	17
	12	0.18	265	250	2.39	17.82
16:1	0	0.22	209	32	1.72	18.34
	2	0.22	223	158	2.79	16.98
	4	0.22	254	242	3.09	16.64
	6	0.22	278	317	3.36	16.41
	8	0.22	287	332	3.3	16.67
	10	0.21	295	285	2.92	17.18
	12	0.19	283	186	2.2	18.23
15:1	0	0.28	261	27	1.77	18.46
	2	0.27	280	123	2.75	17.35
	4	0.28	305	196	3.07	17.09
	6	0.27	325	252	3.19	16.49
	8	0.26	336	242	2.96	17.44
	10	0.23	327	192	2.5	18.09
	12	0.21	306	134	1.99	18.72

Table 3.12: Emissions at various loads and compression ratios for *B30* blend of *SBME* (biodiesel) with diesel oil.

Compression ratio	Load (kg)	CO (%vol)	HC (ppm)	NO (ppm)	CO_2 (%vol)	O_2 (%vol)
18:1	0	0.12	99	96	1.7	18.65
	2	0.11	101	305	2.66	17.29
	4	0.09	104	390	2.83	17.05
	6	0.09	106	406	2.87	17.03
	8	0.08	106	443	2.82	17.05
	10	0.08	106	331	2.41	17.8
	12	0.08	105	248	2.14	18.06
17:1	0	0.16	112	51	1.65	18.63
	2	0.13	110	184	2.59	17.33
	4	0.11	109	211	2.76	17.14
	6	0.1	108	328	2.82	17.08
	8	0.09	109	331	2.67	17.33
	10	0.08	108	305	2.3	17.81
	12	0.08	112	213	1.97	18.35
16:1	0	0.2	139	36	1.66	18.73
	2	0.18	141	105	2.65	17.3
	4	0.16	150	226	2.88	17.22
	6	0.14	152	285	2.87	17.17
	8	0.13	163	287	2.69	17.48
	10	0.12	169	241	2.41	18.03
	12	0.13	178	188	2.1	18.46
15:1	0	0.3	229	28	1.89	18.66
	2	0.27	229	122	2.84	17.52
	4	0.24	231	190	3.09	17.22
	6	0.22	236	255	3.21	17.17
	8	0.25	244	253	2.96	17.56
	10	0.21	257	144	2.68	18.23
	12	0.23	273	101	2.31	18.33

Table 3.13 shows the density and calorific value of soyabean methyl ester at different blending ratios *B10, B20* and *B30* with diesel.

Table 3.13: Density and calorific values of different biodiesel blends.

Serial No.	Blend	Density, (kg/m^3)	Calorific value, (MJ/kg)
01.	B10	767.67	34.112
02.	B20	900	33.311
03.	B30	800	33.742

The Soyabean biodiesel was produced through the process of transesterification and stored in a polyethylene tank for 14 days. The viscosity and calorific values were checked in every four days as the quality parameters under consideration for the biodiesel. The emissions of *B10, B20* and *B30* were measured after the 8th day of storage. Different graphs were plotted to show the variation of quality parameters alteration over the storage period and various emissions at different loads and compression ratios.

- **Variation of kinematic viscosity with storage time:**

With reference from Table 3.7, the graph is plotted between the kinematic viscosity and storage period. With the increase in the storage time, the viscosity of *SBME* sample increases. The reason of this variation is owing to the formation of the peroxide and secondary products like ketones, aldehydes which is due to the oxidation of sample [18]. The variation of the kinematic viscosity with the storage time is shown in figure 3.29.

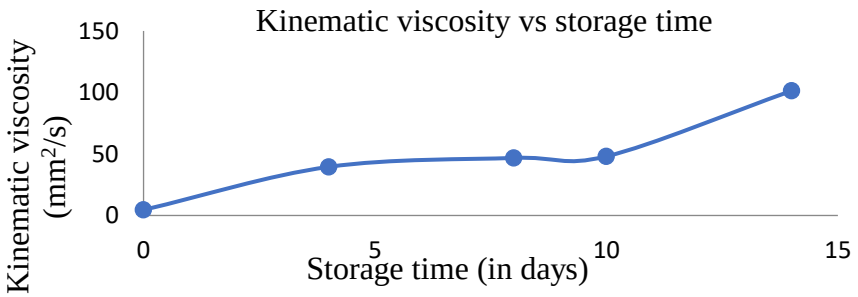

Figure 3.29: Variation of kinematic viscosity with the storage time.

- **Variation of calorific value with storage time:**

With the experimental observations mentioned in Table 3.9, the graph between calorific value and storage time is plotted.

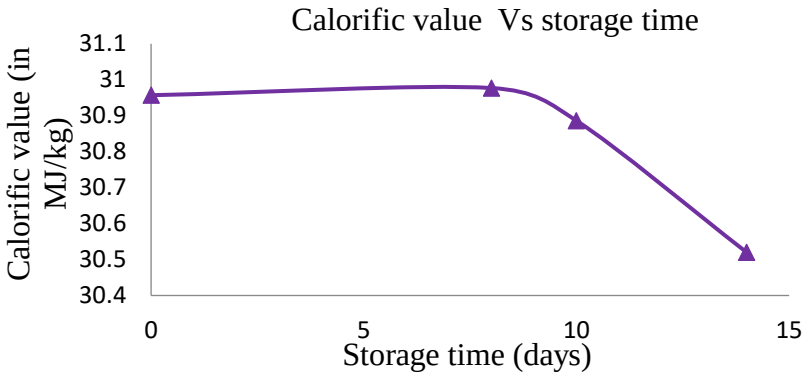

Figure 3.30: Variation of calorific value with storage time.

A marginal decrease in the calorific value of the sample of *SBME* was observed with the storage time in the first 4 weeks, but the value increases to a value greater than the initial reading (Table 3.9). The variation in calorific value with storage time has shown in figure 3.30. The general trend of variation of calorific value of biodiesel with storage time is a decreasing curve. The increase in the calorific value at the end of 8th day of storage is accounted for error in the measurement from the bomb calorimeter equipment.

Larger amounts of water, impurities, and polymers were produced during the storage time and the kinematic viscosity and specific gravity increase with time. As a result, the amount of heat releases from the sample with the storage time. Water produced in biodiesel through the peroxidation chain mechanism, following the occurrence of oxidative instability and hence the amount of water in the samples increased with the extent of oxidative instability. The amount of heat releases thus also decreases with storage time in the samples because of the production of water during the peroxidation chain reaction [18].

- **Emissions at various compression ratios and different load conditions for B10 blend:**

Figure 3.31 indicates that the variation of carbon monoxide with respect to various loads at different compression ratios. It can be seen that the percentage of carbon monoxide in the emissions decreases with increase in the load as well as compression ratio. The amount of carbon monoxide decreases even for the compression ratio 16:1 whose no-load carbon monoxide emission percentage is less than that of 17:1, but with the increase in load, the percentage value carbon monoxide is more for the compression ratio 16:1 than that of 17:1.

Figure 3.32 shows the variation of hydrocarbon concentration with various loads at different compression ratios. It is observed that there is not much variation in the percentage of hydrocarbon at higher loads and at lower compression ratios. It is observed that there is not much variation in the percentage of hydrocarbon at higher loads and at lower compression ratios.

In Figure 3.33, the variation of nitrogen monoxide concentration at various load conditions and different compression ratios are shown. It can be seen that in each case of compression ratio, the concentration of nitrogen monoxide increases with increase in load to a maximum point and then decreases with further increase in load, but the concentration of nitrogen monoxide decreases with decrease in the value of compression ratio. In Figure 3.34, the concentration of carbon dioxide in emission increases to a maximum value and then decreases with increase in load irrespective of compression ratio. It is found that maximum carbon dioxide is emitted at the compression ratio 15:1 and minimum at 16:1. Figure 3.35 describe the variation of oxygen concentration in emission with various loads at different compression ratios. It is reported that for each compression ratio, the profile of variation of the oxygen with increasing load, follows an

upward parabola contour. It can also be seen that the oxygen concentration in the emission is minimum for the compression ratio 17:1 and maximum for 15:1.

Nature of formation of *NO* emissions are different from that of the *CO* and *HC* emissions. High temperature and high compression ratio do not favour *CO* and *HC* emissions. Han et al. [19] studied the emissions of *HC* and *CO* in a premixed low-temperature combustion mode fuelled by blends of diesel and gasoline and investigated the nature of formation of *CO* and *HC*. The formation of *NO* emissions takes place at higher temperature and that is why the *NO* emissions increases with increase in compression ratio. Prompt *NO* form from molecular nitrogen in the air combining with *B10* Soyabean biodiesel blend, which exist, to some extent, in all combustion processes. This nitrogen then oxidizes along with the fuel and becomes *NO* during combustion. As the load increases, temperature inside the engine cylinder increases and hence the rate of formation of *NO* increases up to maximum at load to 6-8 kg but further increase in temperature does not favour *NO* formation due to the formation of many other gaseous emissions like *SOx*. At the same time, at high temperature, Nitrogen and Oxygen molecules offer resistance to come closer to each other due to high value of their kinetic energies. This is in accordance with the kinetic theory of gas.

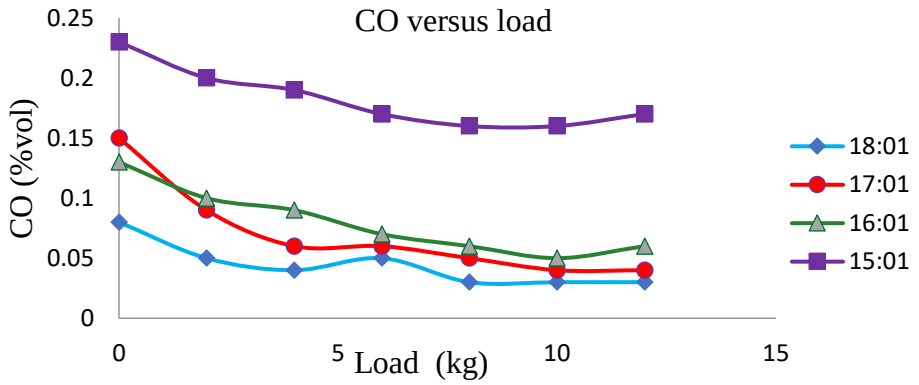

Figure 3.31: Variation of carbon monoxide emission with various loads at different compression ratios for *B10* Soyabean biodiesel blend.

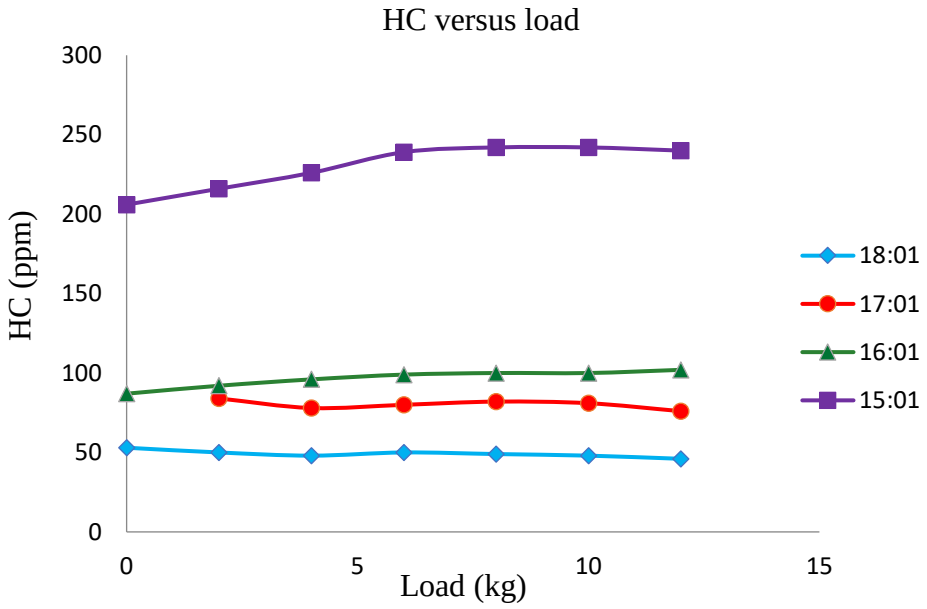

Figure 3.32: Variation of hydrocarbon emission with various loads at different compression ratios for *B10* Soyabean biodiesel blend.

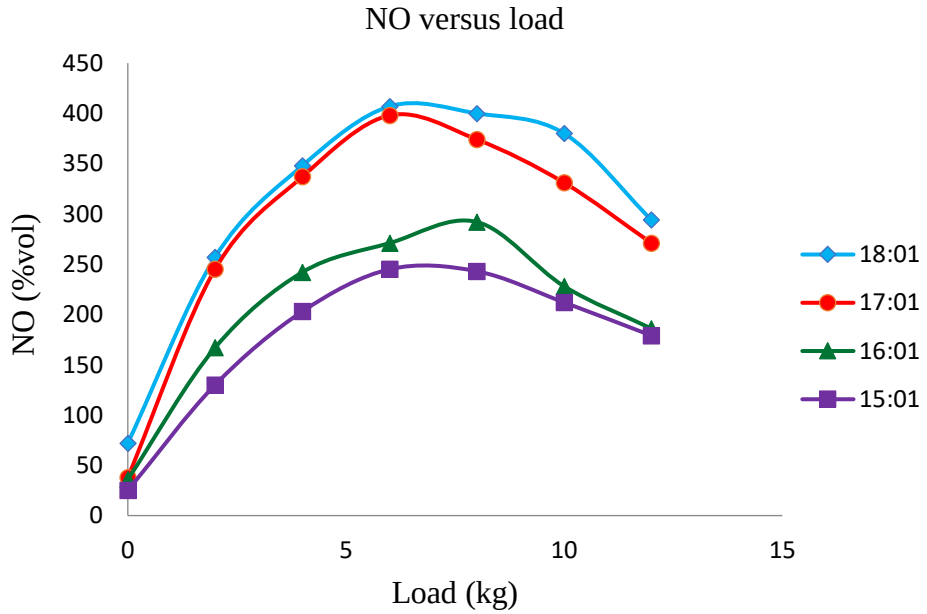

Figure 3.33: Variation of nitrogen monoxide emission with various loads at different compression ratios for *B10* Soyabean biodiesel blend.

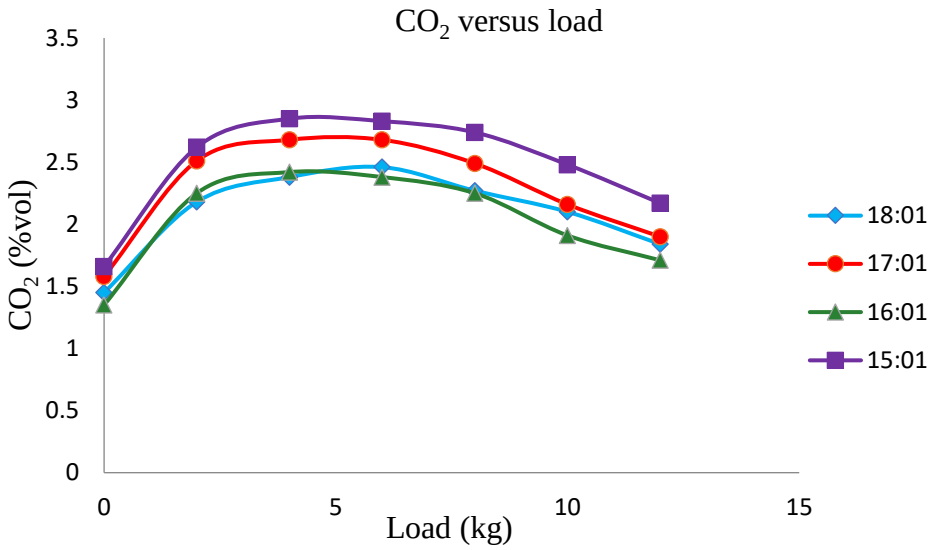

Figure 3.34: Variation of carbon dioxide emission with various loads at different compression ratios for *B10* Soyabean biodiesel blend.

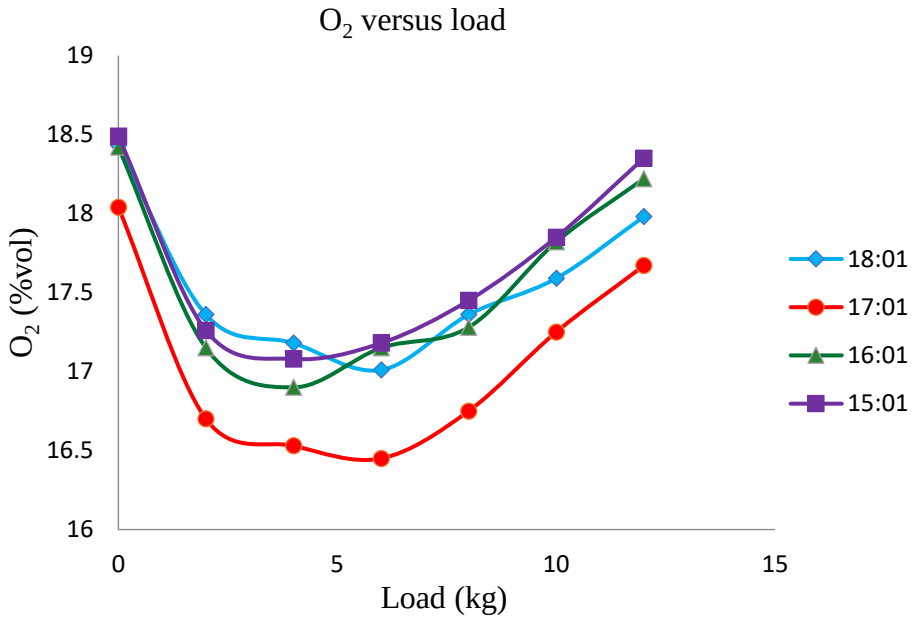

Figure 3.35: Variation of oxygen emission with various loads at different compression ratios for *B10* Soyabean biodiesel blend.

- **Emissions at various compression ratios and different load conditions for B20 blend:**

Figure 3.36 represents the variation of the *CO* emissions at different loads at various compression ratios, and it is observed that not much variation in the value of the *CO* emissions with the load but with respect to compression ratio, 15:1 produces maximum whereas 18:1 the least.

In figure 3.37, the hydrocarbon *(HC)* emissions with different loads at various compression ratios can be observed and can be comprehended that the *HC* emissions are maximum for 15:1 and least for 18:1 compression ratio whereas, with respect to the increasing load, the emission curve is an increasing one irrespective of compression ratio.

Figure 3.38 shows the *NO* emissions, and it is found that it increases with increase in the load to the point of maxima and then decreases with further load increment.

Figure 3.39 shows the CO_2 emissions at various loads and compression ratios, and it can be observed that the emissions increases with increase in load to a certain point and then decreases irrespective of the compression ratio. In figure 3.40, oxygen emission decreases with an increase in load and then it increases with the further increase in the load.

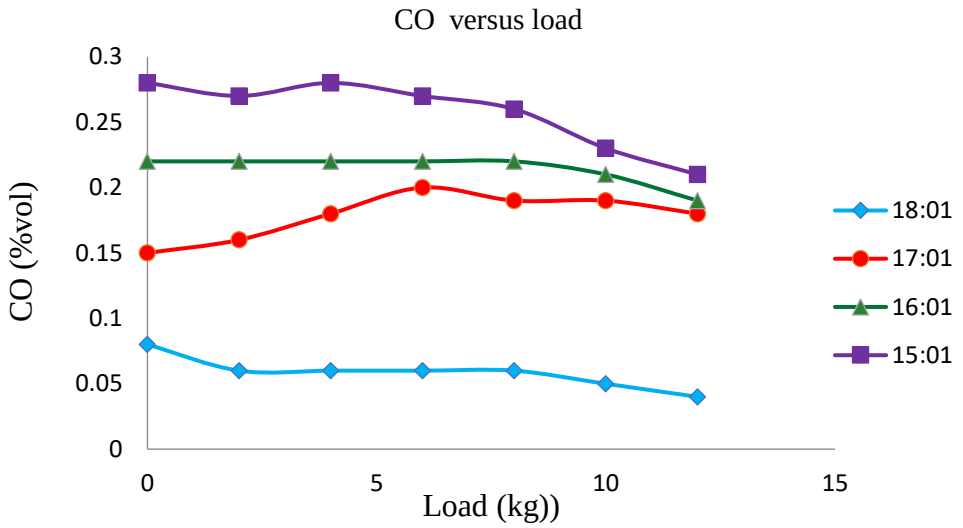

Figure 3.36: Variation of carbon monoxide emission with various loads at different compression ratios for *B20* Soyabean biodiesel blend.

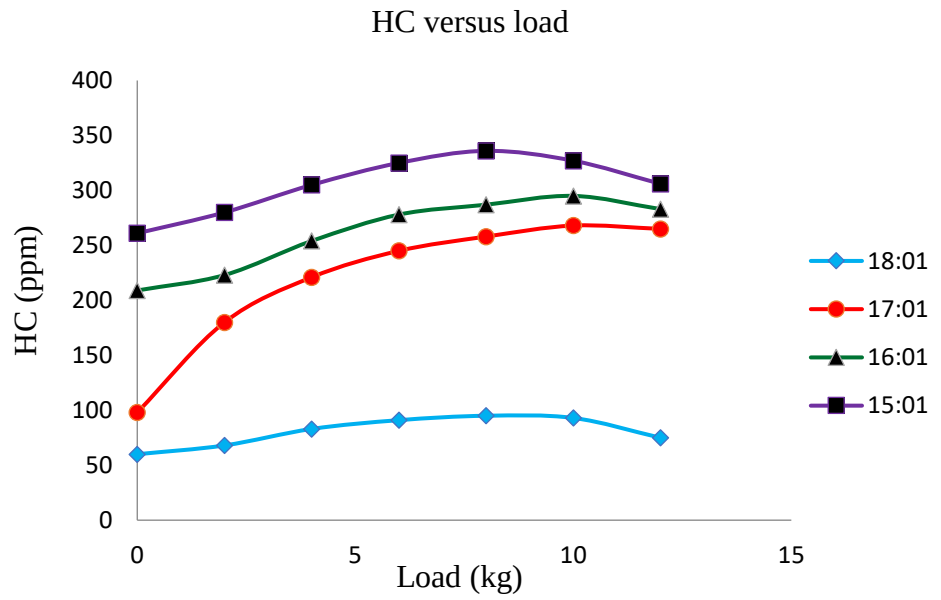

Figure 3.37: Variation of hydrocarbon emission with various loads at different compression ratios for *B20* Soyabean biodiesel blend.

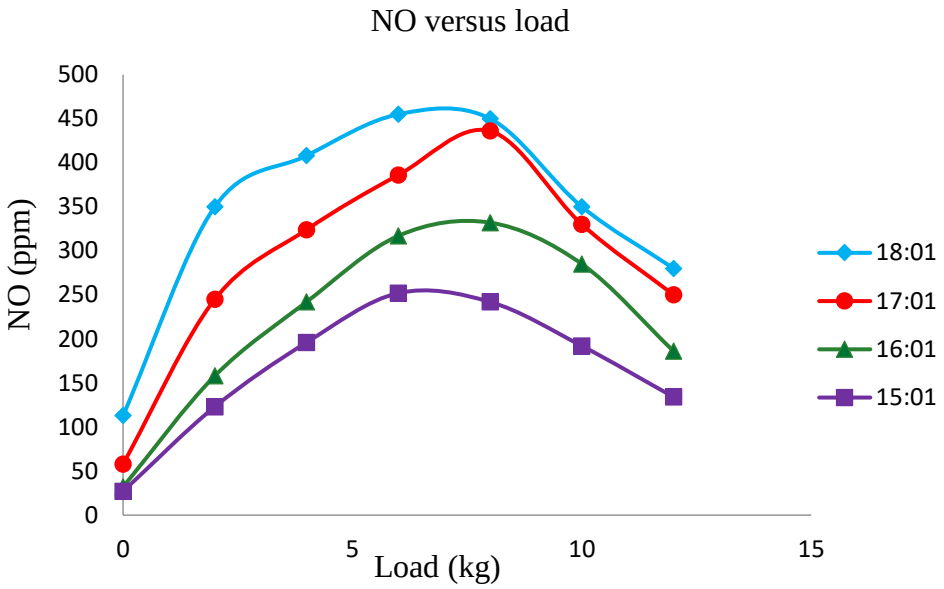

Figure 3.38: Variation of nitrogen monoxide emission with various loads at different compression ratios for *B20* Soyabean biodiesel blend.

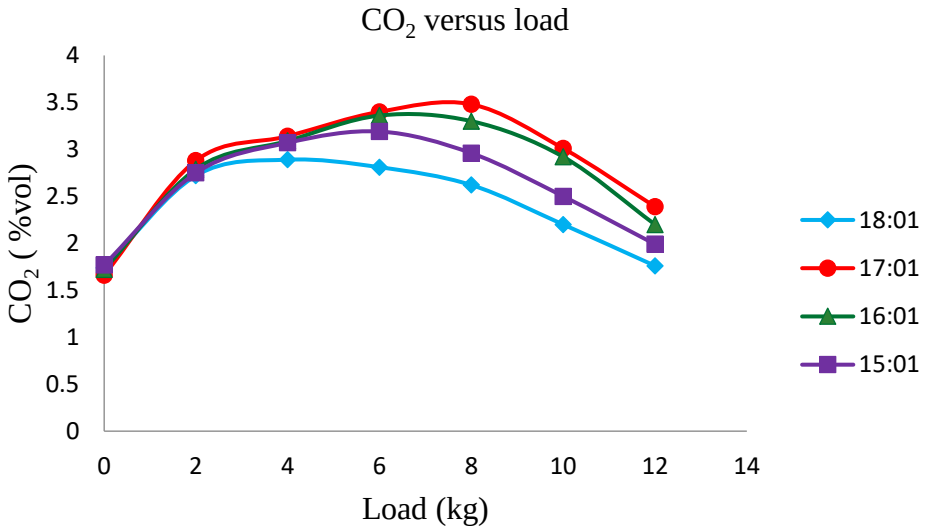

Figure 3.39: Variation of carbon dioxide emission with various loads at different compression ratios for *B20* Soyabean biodiesel blend.

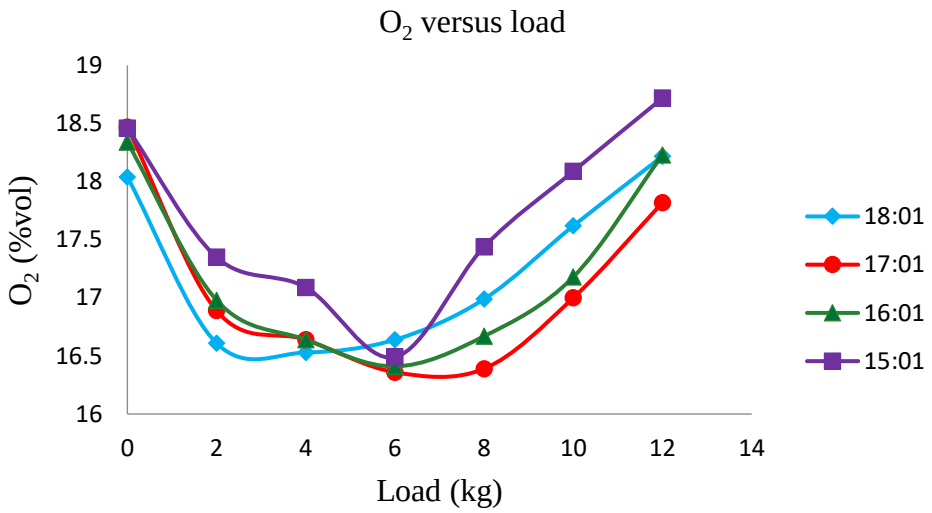

Figure 3.40: Variation of oxygen emission with various loads at different compression ratios for *B20* Soyabean biodiesel blend.

- **Emissions at various compression ratios and different load conditions for B30 blend:**

Figure 3.41 shows the decreasing trend of *CO* emissions with increasing load and the emission decreases with increasing compression ratio. In figure 3.42, it can be seen that there not much alternation in the hydrocarbon *(HC)* content in emission with the increasing load but with an increase in load, the *HC* content decreases.

An increasing curve is noticed for the *NO* content in the emissions with respect to increase load in figure 3.43. Figure 3.44 shows the emission of CO_2 with the increase in load, which is increasing to the point of maxima and then decreases with further increase in load. The opposite trend is seen in oxygen content in emissions as compared to that of CO_2 emissions in figure 3.45.

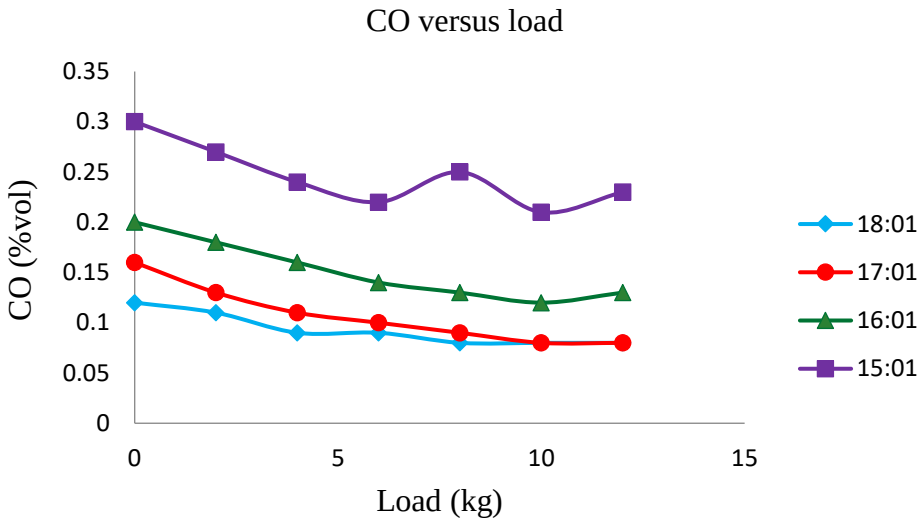

Figure 3.41: Variation of carbon monoxide emission with various loads at different compression ratios for *B30* Soyabean biodiesel blend.

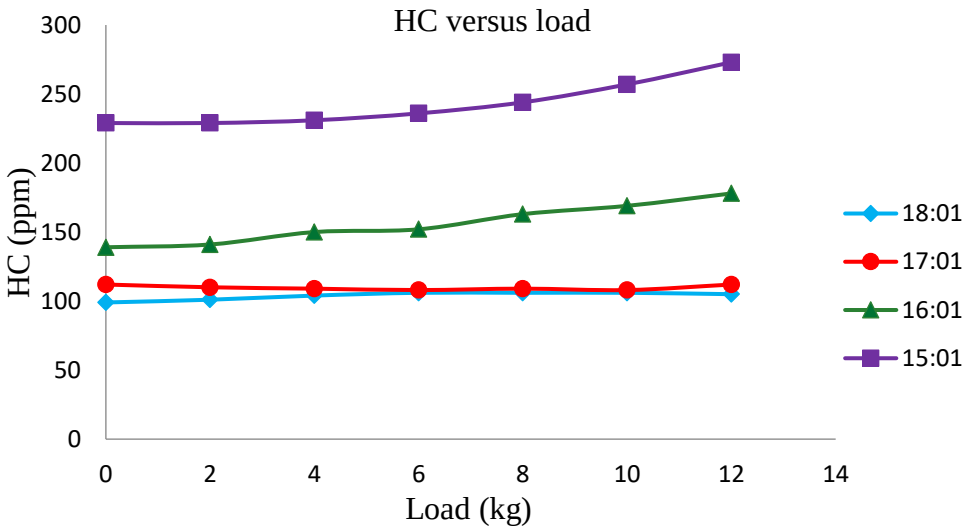

Figure 3.42: Variation of hydrocarbon emission with various loads at different compression ratios for *B30* Soyabean biodiesel blend.

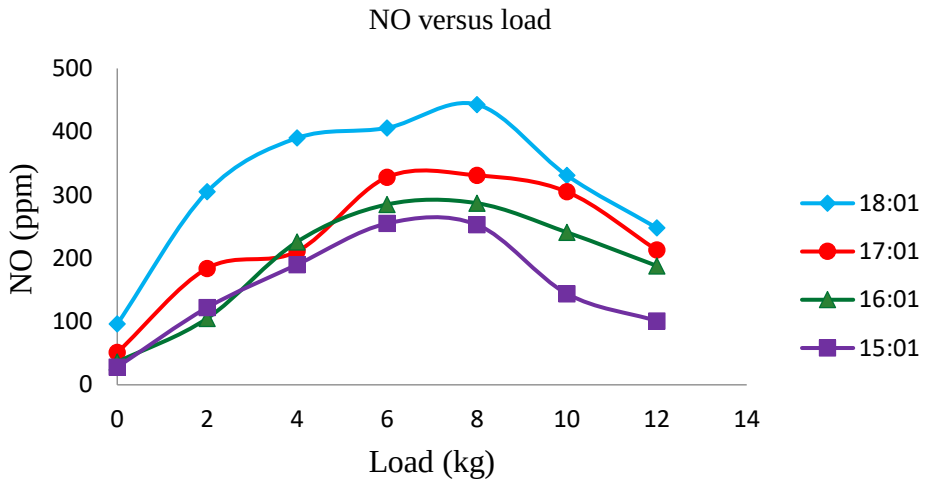

Figure 3.43: Variation of nitrogen monoxide emission with various loads at different compression ratios for *B30* Soyabean biodiesel blend.

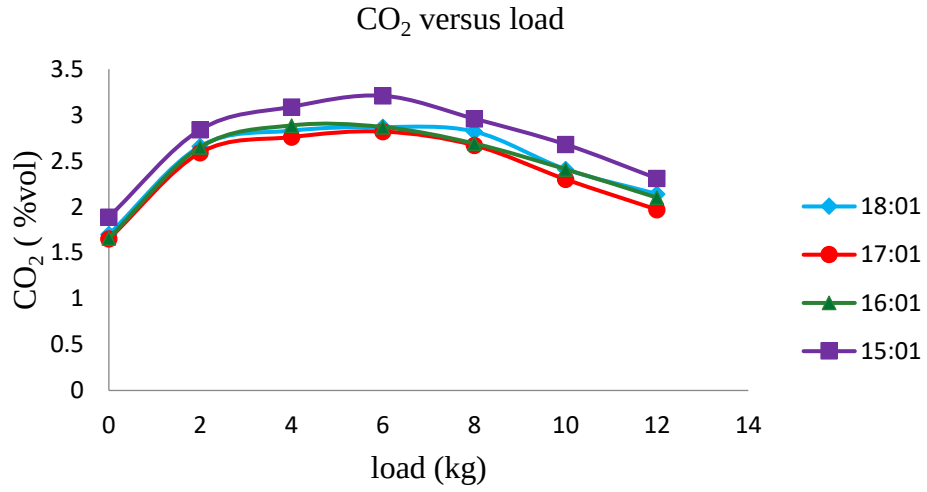

Figure 3.44: Variation of carbon dioxide emission with various loads at different compression ratios for *B30* Soyabean biodiesel blend.

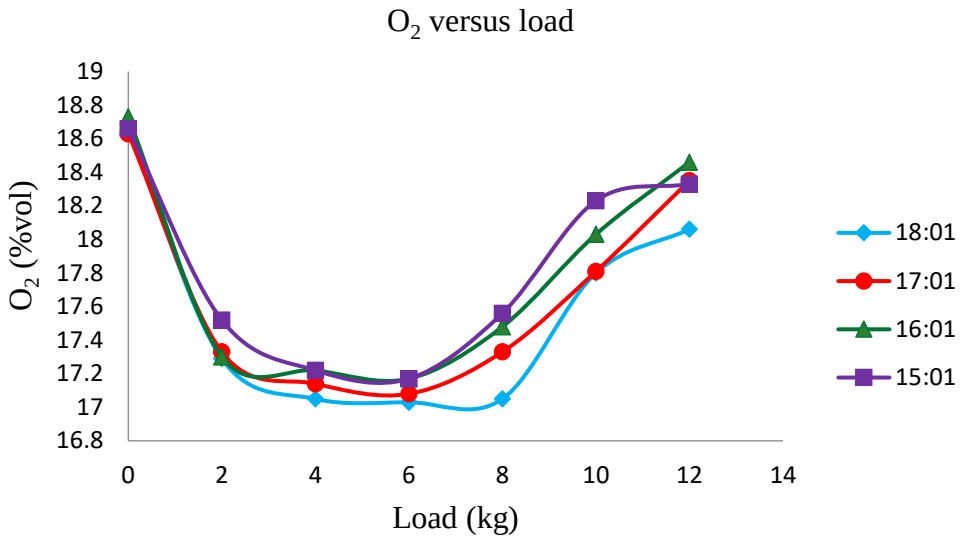

Figure 3.45: Variation of oxygen emission with various loads at different compression ratios for *B30* Soyabean biodiesel blend.

3.8 Conclusions

The quality of producer gas deteriorates due to the presence of dust particles in it. In this context, we used cyclone separator for removing dust particles. Also, we mixed the mineral catalyst calcium oxide with biomass feedstock inside the gasifier system to eliminate the heavy dust particle and tar as well.

The performance of cyclone separator was experimentally investigated for different feedstocks to remove ash and dust particles in producer gas. It was observed:

- that the cyclone collection efficiency decreases after adding the *CaO* from 71.87% to 70.75% for wood feedstock.
- In coconut shell, the cyclone collection efficiency got reduced from 78% to 73.44% due to the quality of inlet gas, which has a lighter particle in it. Leith and Licht model give comparable results with experimental results.

Further biodiesel is blended with conventional diesel in *B10, B20* and *B30* ratios. Following conclusions are drawn by conducting the mentioned experiments on biodiesel.

- The kinematic viscosity of the biodiesel increases with storage time. This is due to the formation of different oxidized products, including hydroperoxides and aldehydes, ketones etc.
- The calorific value of the biodiesel drops down at a slow rate for the observational intervals of 2-4 days. Therefore, the storage time affects the calorific value of the biodiesel.
- The carbon monoxide content in the emission decreases with the increase in the load, while the hydrocarbon content remains nearly constant. Nitrogen monoxide and carbon dioxide content increase with an increase in load to a particular point of maxima and then decreases with further increase in the load. The oxygen content shows exactly the opposite behaviour with respect to carbon dioxide.

The nature of the emission curve for *B10, B20* and *B30* curve remains similar for different loads at various compression ratios.

References

[1] A. K. Rajvanshi, Director, Nimbkar Agricultural Research Institute," Biomass Gasification," pp. 3-7.

[2] P. Hasler and T. Nussbaumer, " Gas cleaning for IC engine applications from fixed bed biomass gasification". Journal of Biomass and Bioenergy, Vol. 16, pp. 385-395, 1999.

[3] H. Jun, and K. Heejoon, “The reduction and control technology of tar during biomass gasification/pyrolysis: An overview,” Journal of Renewable and Sustainable Energy Reviews, Vol. 12, pp. 397-416, 2008.

[4] "Air pollution control technology fact sheet", EPA-452/F-03-005, pp. 3-4.

[5] https://en.wikipedia.org/wiki/Cyclonic_separation, accessed on November 24, 2019.

[6] P. A. Funk and K. D. Baker, " Engineering and Ginning Dust Cyclone Technology – A Literature Review". The Journal of Cotton Science, Vol. 17, pp. 40–51, 2013.

[7] M. Rhodes," Introduction to Particle Technology"2nd edition, John Wiley & Sons Ltd. ISBN: 978-0-470 -01427-1, pp. 250-255, 2008.

[8] C. R. Wilke, " A viscosity equation for gas mixtures," The Journal of Chemical Physics, Vol. 18. Number-4, April, 1950.

[9] N. d. Charisiou, G. J. Tsevrenis and M. A. Goula, "Software development for the design of control equipment for particulate pollutants", 12th International conference on environmental science and technology, Rhodes Greece, 8-10 September 2011.

[10] L. Wang, C. B. Parnell, B. W. Shaw and R. E. Lacey, "A theoretical approach for predicting number of turns and cyclone pressure drop", American Society of Agricultural and Biological Engineers, Vol. 49 (2), pp. 491−503, 2006.

[11] L.C. Meher, D. V. Sagar and S. N. Naik, “Technical aspects of biodiesel production by transesterification—a review,” Renewable and Sustainable Energy Reviews, Vol. 10, pp. 248-68, 2006.

[12] S. Jaichandar and K. Annamalai, “The Status of Biodiesel as an Alternative Fuel for Diesel Engine– An Overview,” Journal of Sustainable Energy & Environment, Vol. 2, pp. 71-75, 2011.

[13] D. Viesturs and L. Melece, “Advantages and Disadvantages of Biofuels: Observations in Latvia,” Engineering for Rural Development, 2014.

[14] F. Ma and M. A. Hanna, “Biodiesel production: a review,” Bioresource Technology, Vol. 70, pp. 1-15, 1999.

[15] A. K. Agarwal, and T. P. Bajaj, “Process optimisation of base catalysed transesterification of Karanja oil for biodiesel production,” *Int. J. Oil, Gas and Coal Technology*, Vol. 2, No. 3, pp. 297–310, 2009.

[16] A. K. Agarwal and D. Khurana, “Long-term storage oxidation stability of Karanja biodiesel with the use of antioxidants,” Fuel Processing Technology, Vol. 106, pp. 447-52, 2013.

[17] S. S. Damasceno, N. A. Santos, I. M.G. Santos, A. L. Souza, A. G. Souza, and N. Queiroz, “Caffeic and ferulic acids: An investigation of the effect of antioxidants on the stability of soybean biodiesel during storage,” Fuel, Vol. 107, pp. 641-46, 2013.

[18] A. khalid N. Tamaldin, M. Jaat, M.F.M. Ali, B. Manshoor and I. Zaman, “Impacts of biodiesel storage duration on fuel properties and emissions,” Procedia Engineering, Vol. 68, pp. 225-30, 2013

[19] D. Han, A. M. Icker, S. V. Bohac, Z. Huang, and D. N. Assanis, “HC and CO emissions of premixed low-temperature combustion fueled by blends of diesel and gasoline,” Fuel, Vol. 99, pp. 13-19, 2012.